




# Visualizing and quantifying molecular and cellular processes in *Caenorhabditis elegans* using light microscopy

Pavak Shah ,<sup>1,2,\*</sup> Zhirong Bao ,<sup>3,\*</sup> Ronen Zaidel-Bar <sup>4</sup>

<sup>1</sup>Department of Molecular, Cell, and Developmental Biology, University of California Los Angeles, Los Angeles, CA 90095, USA,

<sup>2</sup>Institute for Quantitative and Computational Biosciences, University of California Los Angeles, Los Angeles, CA 90095, USA,

<sup>3</sup>Developmental Biology Program, Sloan Kettering Institute, New York, NY 10065, USA,

<sup>4</sup>Department of Cell and Developmental Biology, Faculty of Medicine, Tel Aviv University, Tel Aviv 6997801, Israel

\*Corresponding author: Department of Molecular, Cell, and Developmental Biology, University of California Los Angeles, Los Angeles, CA 90095, USA. Email:

pavak@g.ucla.edu; \*Corresponding author: Developmental Biology Program, Sloan Kettering Institute, New York, NY 10065, USA. Email: baoz@mskcc.org

## Abstract

Light microscopes are the cell and developmental biologists' "best friend," providing a means to see structures and follow dynamics from the protein to the organism level. A huge advantage of *Caenorhabditis elegans* as a model organism is its transparency, which coupled with its small size means that nearly every biological process can be observed and measured with the appropriate probe and light microscope. Continuous improvement in microscope technologies along with novel genome editing techniques to create transgenic probes have facilitated the development and implementation of a dizzying array of methods for imaging worm embryos, larvae, and adults. In this review, we provide an overview of the molecular and cellular processes that can be visualized in living worms using light microscopy. A partial inventory of fluorescent probes and techniques successfully used in worms to image the dynamics of cells, organelles, DNA, and protein localization and activity is followed by a practical guide to choosing between various imaging modalities, including widefield, confocal, lightsheet, and structured illumination microscopy. Finally, we discuss the available tools and approaches, including machine learning, for quantitative image analysis tasks, such as colocalization, segmentation, object tracking, and lineage tracing. Hopefully, this review will inspire worm researchers who have not yet imaged their worms to begin, and push those who are imaging to go faster, finer, and longer.

**Keywords:** fluorescence microscopy; confocal microscopy; lightsheet microscopy; green fluorescent protein; image analysis; super resolution; molecular dynamics; activity sensors; localization; spatiotemporal resolution; WormBook

## Introduction

We are visual creatures, which is why for us "seeing is believing"; the ability to visualize molecular and cellular processes taking place inside the worm enhances our ability to understand them. Since the worm is mostly transparent, it opens up many options for light microscopy to illuminate its inner workings. As will be discussed below, imaging the native worm with differential interference contrast (DIC) microscopy remains a useful option for some applications, but more often than not we will introduce into the worm a fluorescent probe and use fluorescence microscopy to gather quantitative information about its intensity and localization. The type of probe and imaging modality depend on the biological question at hand. For example, "Where is gene X expressed?" or "Where is protein X localized?" are questions that require different probes to answer, and "How fast does cell X migrate?" or "For how long is TF X bound to DNA?" are questions that can require different imaging modalities to answer. This chapter is divided into 3 sections. In the first, we will review some of the most commonly used methods to visualize what is

happening inside the worm, highlighting various fluorescent probes. The next section will focus on the microscopes and imaging modalities, and in the final section we will address how imaging data can be processed in a quantitative way.

## Probes

We will introduce the various imaging probes according to the cellular compartment they serve to elucidate. This information is summarized in graphic form in Fig. 1 and a few examples are shown in Fig. 2. A list of commonly used fluorescent proteins (FPs) in *Caenorhabditis elegans* is provided in Table 1, and a companion collection is available from the FPbase which provides more detailed information for each (<https://www.fpbase.org/col/lection/1827/>).

## Cell morphology and position

The seminal work of Sulston *et al.*, mapping out the entire lineage of the developing worm, was performed using Nomarski-type DIC

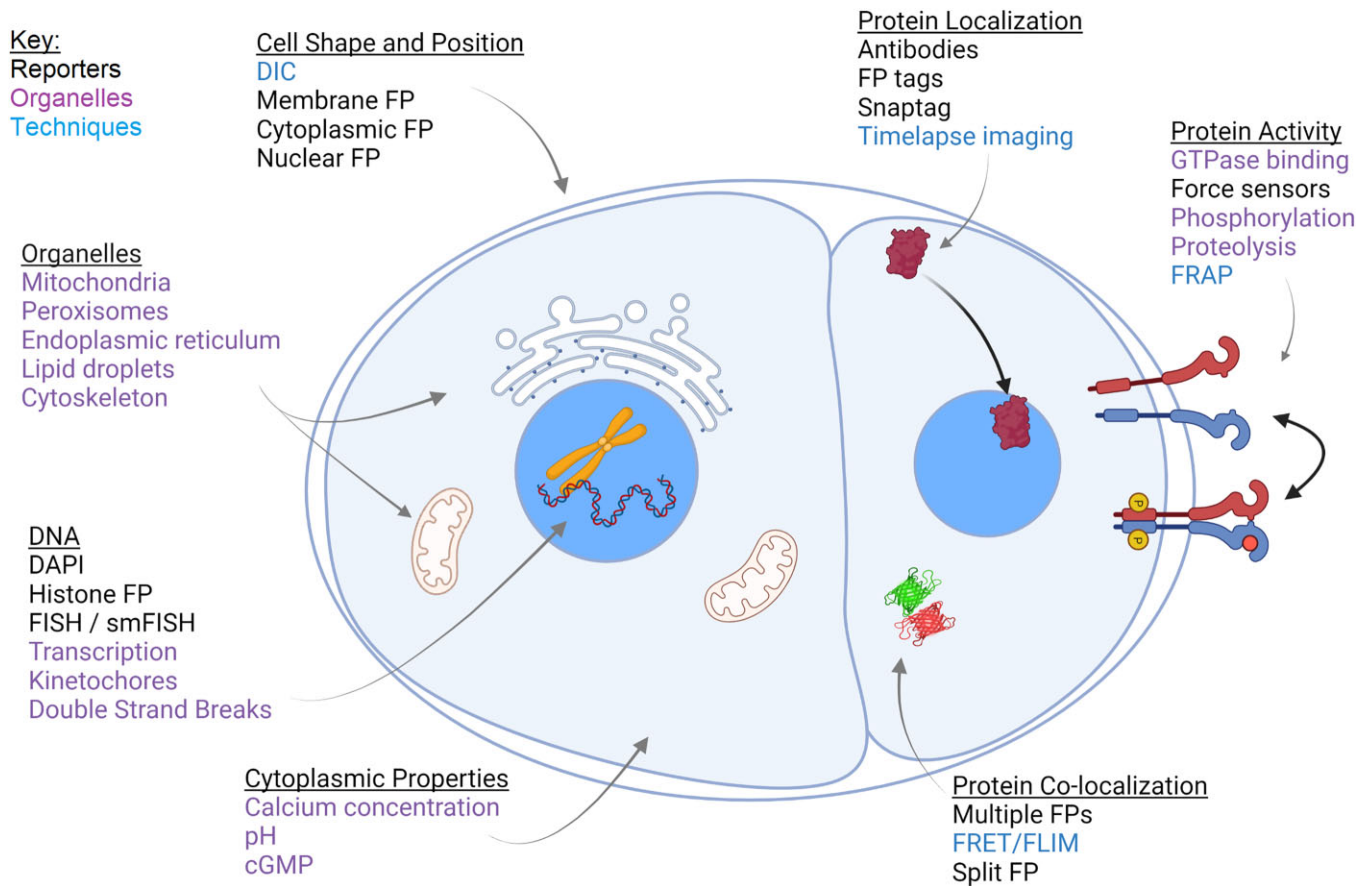


**Fig. 1.** Visualizing the inner workings of *C. elegans* with fluorescence microscopy. The methods and probes listed here and described in detail in the Introduction of the text give us the ability to measure properties and follow dynamics at the protein, organelle, and cellular level within living worms.

microscopy (Sulston et al. 1983). Taking advantage of inherent differences in the optical density of various regions of the cells, it is easy to discern the nucleus and cell–cell junctions, as well as granules within cells, using polarized white light. DIC is still a good option for following morphogenesis and apoptosis during embryogenesis, because the imaging conditions do not generally induce notable phototoxicity and any genetic background can be imaged without the need to introduce an external probe. However, marking the nuclei with a fluorescent probe, such as GFP::Histone (GFP: green FP) can make lineaging much easier and facilitates automatic identification and lineaging, as discussed in Image analysis. Furthermore, if it is important to trace the exact cell morphology then DIC is not sufficiently accurate and a fluorescent plasma membrane marker, such as a plekstrin homology domain fused to GFP (Audhya et al. 2005), or a cytoplasmic FP should be expressed.

### Protein localization

To find out where in the worm a given protein localizes, immunostaining with a specific antibody is possible, but suffers from several drawbacks, namely scarcity of suitable antibodies, fixation artifacts and an inability to resolve dynamics. The major advantage of immunolabeling over FP tagging, i.e. observing the endogenous protein, has been largely eliminated by CRISPR-cas9-mediated genome editing, which allows tagging of the endogenous protein with an FP. That said, a good antibody still has the advantage of high sensitivity due to the amplification of signal by multiple secondary antibodies binding each primary antibody.

With the pioneering work of Chalfie, the worm was instrumental in the development of GFP as a means to follow protein expression in transgenic animals (Chalfie et al. 1994; Yang et al. 1996). The first GFP-tagged protein was made in *Drosophila* (Wang and Hazelrigg 1994), but since then, thousands of worm proteins have been tagged with a FP (usually GFP), catapulting forward the fields of cell and developmental biology (Fig. 2a). Moreover, since the advent of CRISPR-Cas9 as a tool for genome editing (Chen et al. 2013; Chiu et al. 2013; Dickinson et al. 2013; Friedland et al. 2013; Katic and Großhans 2013; Lo et al. 2013; Tzur et al. 2013; Waaijers et al. 2013), hundreds of worm proteins have been tagged at their endogenous loci (many of them available at the CGC). Despite being expressed from only 2 copies, the fluorescent intensity of endogenously tagged proteins is not necessarily lower than that of ectopic transgenes, which can contain hundreds of copies of the gene, and in some cases they are brighter, probably because they are not silenced as transgenes often are (Dickinson et al. 2013).

When engineering the fusion of an FP to a novel protein of interest one needs to consider where the FP is least likely to affect the protein's function. If the structure of the protein is known it should be consulted. Generally, C-terminal fusions with an appropriate linker for flexibility often work, but if the business end of the protein is at its C-terminus then an N-terminal fusion is preferable. When inserting an FP into the endogenous locus one also needs to consider splice variants; if tagging all variants is desired this will often limit the choice of insertion site. In some instances, both C- and N-termini of the protein have important functions, in which case it is necessary to insert the FP within

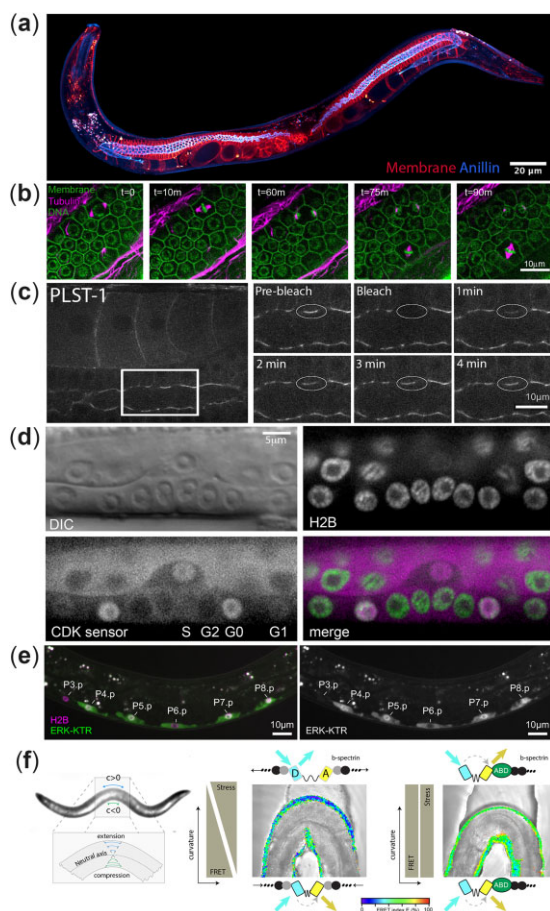


**Fig. 2.** Examples of visualizing molecular and cellular processes in *C. elegans* using fluorescently tagged proteins. a) Three-dimensional architecture of the germline highlighted by a Z-stack projection of an adult hermaphrodite expressing a PH domain fused to mCherry as a membrane marker (red) and ANI-2::GFP localized at rachis bridges (blue). The fluorescent markers are expressed exclusively in the germline. Image credit: Priti Agarwal. b) Mitotic cell divisions in the distal end of the germline captured by time-lapse microscopy of an immobilized hermaphrodite expressing mKate2::TBA-1 to mark MTs (magenta), HIS-72::GFP to mark DNA (green), and GFP:PH to mark the plasma membranes (green). Images are time stamped (in minutes) from first frame. Image credit: Anat Nitzan. c) Molecular dynamics of actin binding protein PLST-1 revealed by the rate of recovery after photobleaching. PLST-1::GFP in the syncytial germline is bleached by strong laser on a small region of the rachis (marked by oval) and fluorescence recovery, followed by time-lapse imaging, reports on protein turnover rate. Image credit: Shinjini Ray. d) Ubiquitous expression of a ratiometric CDK sensor can be used to predict cell cycle states based on CDK activity. Single plane confocal images of *rps-27p::DHB::2xmKate2::P2A::H2B::GFP* of an L3 stage animal showing uterine-vulval development. Interphase state predictions based on CDK sensor localization are annotated beneath the vulval precursor cells in the gray scale image below the DIC image (left), nuclear mask used for quantification (H2B, top right) and overlay (bottom right). Image credit: Jayson Smith and David Matus. e) In vulval precursor cells (VPCs), the ERK activity biosensor ERK-KTR (green) is excluded from the nucleus (marked by histone H2B, magenta) of P6.p, a cell where MPK-1 activation is high. ERK-KTR is enriched in nuclei of P4.p, P5.p, P7.p, and P8.p, cells where MPK-1 activation is low. Image credit: Claire de la Cova. f) Genetically encoded mechanical tension sensor based on a FRET tension module inserted within b-spectrin. The bending stresses in a worm trapped in a curved microfluidic device are visualized by FRET (middle). As a negative control, a tension sensor module fused to the N-terminus of b-spectrin, which cannot be pulled apart and hence does not respond to curvature induced stresses was used (right). Blue pixels indicate low FRET efficiency and strong donor emission, green/yellow pixels indicate high FRET efficiency and strong acceptor emission (after excitation of the donor). c, curvature; D, donor; A, acceptor; ABD, actin binding domain. Image credit: Michael Krieg.

some internal loop region. In the rare cases where nowhere along the protein can an FP be introduced without perturbing its function a smaller tag, such as SNAP-tag could be tried (Maduzia et al. 2011; Aoki et al. 2021). Otherwise, antibody staining might be the only option.

Regarding the FP itself, there is a wide range of options across the visible spectrum (see <https://www.fpbases.org/>), although for single color imaging enhanced GFP (EGFP) is still the first choice in most cases. Other commonly used FPs in worms include yellow FP (YFP), mNeonGreen, mApple, mCherry, mKate2, mScarlet, and TagRFP (RFP: red FP). An overview of FPs used in worms can be found in the review by Breimann et al. (2019) and in Table 1. Note that fusion protein functionality can be affected, for example, due to FP aggregation, by some but not other FPs. Therefore, if a fusion protein mis-behaves it is worth trying a different FP, preferably a monomeric variant. The brightness of an FP in the worm does not always match predictions based on in vitro measurements and they vary in their photostability as well (Heppert et al. 2016). When adapting a new FP for expression in *C. elegans*, there are several genetic engineering rules, pertaining to codon usage, intron inclusion, promoter, and 3'UTR, which should be followed to optimize expression and avoid silencing in the germline (reviewed in Nance and Frøkjær-Jensen 2019).

It is possible to express separately 2 complementary parts of an FP and when they meet in the cell they combine to form a functional FP (Hu et al. 2002). This technique, called bimolecular fluorescence complementation, was adapted in the worm to facilitate tissue-specific labeling of endogenous proteins. The larger fragment of the FP (split-GFP or split-wrmScarlet) is expressed ubiquitously or under a tissue-specific promoter, while the smaller fragment is inserted into the genome to tag the protein of interest, using CRISPR-Cas9 (Goudeau et al. 2021). To increase the brightness of endogenously tagged proteins it is possible to fuse up to 7 tandem copies of the small FP fragment (He et al. 2019).

An important fact to be aware of while imaging fluorescently tagged proteins in *C. elegans* is that even without any labeling certain structures in the worm will fluoresce at all visible wavelengths. The strongest autofluorescence is exhibited by intestinal gut granules, and it can also be observed in hypodermal nucleoli, the cuticle, and the vulva. The autofluorescence of gut granules can actually be used as a noninvasive bio-marker of senescence and advanced glycation end products (Pincus et al. 2016; Komura et al. 2021). However, if the autofluorescence interferes with the visualization of an FP fusion protein, there are a few solutions. Teuscher et al. describe a triple band GFP filter set that separates the GFP signal from autofluorescence (Teuscher and Ewald 2018). Alternatively, it is possible to acquire an image at a wavelength not occupied by the FP and then subtract its fluorescence from the FP image. Finally, gut granule loss (*glo*) mutants are available, but they deviate from the wild-type in other ways as well (Hermann et al. 2005).

## Protein colocalization

A few visual methods exist to test whether 2 or more proteins are situated adjacent to each other. The simplest is 2-color or multi-color imaging. One must choose FPs with emission wavelengths that are separable by the microscope being used. Some examples of pairs of FPs are: Cyan FP (CFP) and YFP, GFP and mCherry, and mScarlet and nNeonGreen. Three color imaging can be done by adding tagBFP (BFP: blue FP) on the blue end of the spectrum (Chai et al. 2012) or CemOrange2 in between red and green emitters (Thomas et al. 2019). If the signals from the 2 proteins are distinct in terms of wavelength, yet they overlap in terms of cellular



**Table 1.** Common fluorescent proteins used in *C. elegans* imaging.

Fluorescent protein	Excitation (nm)	Emission (nm)	Oligomerization	Source or reference	Notes
mTagBFP2	399	454	Monomer	Addgene #122255	
Cerulean	433	475	Weak dimer	Addgene #122250	1
CFP	456	480	Dimer	Addgene #27510	
mTFP	468	495	Monomer	Addgene #122254	
eGFP	488	507	Weak dimer	Addgene #1494	
Dendra2	490/553	507/573	Monomer	Addgene #159803	2
Kaede	508/572	518/580	Tetramer	Ando et al. (2002)	2
mNeonGreen	506	517	Monomer	Addgene #159799	3
eYFP	513	527	Weak dimer	Addgene #27505	4
Venus	515	528	Weak dimer	Addgene #37464 <sup>a</sup>	5
Ypet	517	530	Weak dimer	Addgene #66824	6
mKO2	551	565	Monomer	Addgene #122252	7
tdTomato	554	581	Tandem dimer	Addgene #84830 <sup>a</sup>	
TagRFP-T	555	584	Monomer	Addgene #122256	
mScarlet-I	569	593	Monomer	El Mouridi et al. (2017)	8
mCherry	587	610	Monomer	Addgene #19328	9
mKate2	588	633	Monomer	Addgene #91825 <sup>a</sup>	
mNeptune2.5	599	643	Monomer	Yemini et al. (2021)	
mCardinal	604	659	Monomer	Addgene #159801	

<sup>a</sup> Plasmids that are not simple promoter-fusion expression constructs.

<sup>1</sup> Newer variants exist, but not widely used in worms.

<sup>2</sup> Red/Green photoconvertible.

<sup>3</sup> Can be imaged using filters for green or yellow FPs.

<sup>4</sup> Often referred to as simply "YFP."

<sup>5</sup> Brighter derivative of eYFP.

<sup>6</sup> Brighter derivative of Venus.

<sup>7</sup> Long Stokes shift, can be excited at 488.

<sup>8</sup> Fast folding variant of mScarlet, worm-optimized.

<sup>9</sup> Monomeric but prone to aggregation.

space, they can be said to colocalize. However, with the spatial resolution of an ordinary microscope, they could still be hundreds of nanometers apart, or more if chromatic aberrations are not fully corrected. Super resolution microscopy methods (see *Microscopy*) can reduce the threshold for perceived colocalization down to tens of nanometers. The use of split-FPs, such as split-GFP can provide proof that 2 proteins are within "touching distance." An FP is split in 2 and each fragment is fused to one of the 2 proteins being investigated. Only if and where the 2 proteins are in direct contact will the complete FP assemble and fluoresce. This can also be done on the extracellular domains of proteins to detect synapse formation, where the method is referred to as GRASP (Feinberg et al. 2008).

Another method to detect very close proximity is fluorescence resonance energy transfer (FRET). This method works with specific pairs of FPs in which the emission energy of 1 FP is in the right range to excite the other FP and therefore when illuminating with the excitation wavelength of 1 FP one can observe emission of the other FP, providing the 2 FPs are within fewer than 10 nm from each other. Since FRET occurs at the single molecule level but we observe emissions from numerous molecules simultaneously, the accurate interpretation of FRET experiments requires many controls and careful quantification (Kaminski et al. 2014). The ratiometric nature of FRET in particular limits the effective dynamic range of the method, especially when either of the FP pair is present at higher concentration or is significantly brighter. A variation of FRET that is not sensitive to protein concentrations is fluorescence lifetime imaging microscopy (FLIM), in which a shortening in the fluorescence lifetime of the donor FP is expected only if the acceptor FP is within 10nm or less. Llères et al. used quantitative FRET-FLIM to monitor nanoscale chromatin compaction in germ cells (Llères et al. 2017). Devkota et al. used FRET between GFP and mCherry to show that the interaction between the 2 components of the adiponectin receptor (PAQR-2 and

IGLR-2) is regulated by membrane fluidity (Devkota et al. 2021). Herbet et al. used FRET between GFP- and mCherry-labeled histones to measure the relative compaction of chromatin in the germline under various genetic backgrounds (Herbet et al. 2020). In cases where the underlying interaction being measured by FRET occurs on timescales approaching the frame rate of the imaging itself, simultaneously capturing images in both channels may be necessary to avoid artifacts. This is typically achieved by using 2 detectors or by using optics to project each channel side by side onto a single sensor. While the first approach can be costlier, it preserves the maximum field of view of the microscope. Multicolor splitters can be less costly than advanced scientific cameras, but introduce aberrations into the image that cannot be fully corrected in optics.

## Protein dynamics and activity

For some proteins, location is paramount. For example, a transcription factor can only be active in the nucleus and a cell–cell adhesion receptor can only do its job at cell–cell junctions. Therefore, a change in protein localization is often associated with a change in its activity. To follow protein localization dynamics one can perform time-lapse imaging (Fig. 2b). When planning live-worm time-lapse experiments, one needs to take into consideration the required temporal and spatial resolution and find an optimum that minimizes the exposure of the animal to high intensity light because of the deleterious effects of free radicals generated during the excitation of FPs or dyes (phototoxicity). Live-worm imaging requires compromising on the signal to noise ratio in order to keep the worm alive. Imaging of protein dynamics in early embryos is relatively straightforward because the embryos do not move (Bao and Murray 2011). Concurrent with embryo elongation, muscle twitching begins, and imaging becomes more challenging, but still possible (Lardennois et al. 2019). However, imaging at subcellular resolution within larva or adults requires their temporary immobilization, an additional

complication for which several techniques have been developed (Rohde and Yanik 2011; Gritti et al. 2016; Churgin et al. 2017; Keil et al. 2017; Suzuki et al. 2019; Berger et al. 2021; Mondal et al. 2021; Spiri et al. 2022).

Another type of protein dynamics that can be probed with fluorescent fusion proteins is the turnover within a cellular structure. For example, a cytoskeletal structure, such as the rachis inside the syncytial germline, can remain stable for the worm's lifetime while its protein components continuously exchange with the cytoplasmic pool (Priti et al. 2018). To quantify the rate of protein turnover within the structure one can perform fluorescent recovery after photobleaching (FRAP). In such an experiment, a strong and localized pulse of laser bleaches the fluorescently tagged proteins within the targeted structure and then the recovery is followed by time-lapse imaging (Fig. 2c). The recovery of fluorescence is a direct measure of the turnover of bleached protein from within the structure and its exchange with unbleached FPs from other regions of the cell [e.g. Lantzsch et al. (2021)]. FRAP can also be used to measure membrane fluidity with a prenylated GFP (Devkota and Pilon 2018) and if all the proteins in the cell are bleached at once then FRAP can be used to quantify protein synthesis rates (Papandreou et al. 2020).

Seeing where a protein is localized is not always sufficient to understand its function because the protein might have an active and inactive state; therefore, a method to visualize its active state or the product of its activity is more informative. Several such protein activity reporters have been developed or adapted for worms. A few examples will be given here, but with imagination, ingenuity and a fair amount of trial-and-error experiments many more protein activity reporters can be engineered.

One type of kinase activity sensors is based on phosphorylation inhibiting a nuclear localization signal and enhancing an export signal, thus converting kinase activity into a shifting of the nuclear to cytoplasm ratio of a kinase-specific substrate fused to an FP. For example, to follow cell cycle entry a CDK activity sensor was developed (Spencer et al. 2013). It consists of a DNA Helicase fragment with nuclear export and import signals fused to GFP. When the CDK-cyclin complex is activated the sensor becomes phosphorylated and translocates from the nucleus to the cytoplasm (Fig. 2d). The shift in nuclear to cytoplasmic ratio of GFP is a direct readout of CDK activation and was used to visualize the moment of cell cycle entry in dividing seam cells during *C. elegans* larval development (van Rijnberk et al. 2017).

A similar approach was used to adapt a mammalian ERK sensor to visualize the ERK ortholog MPK-1 in several cell types and different developmental processes in *C. elegans* (Fig. 2e). In this case, an ERK substrate fused to mClover was expressed from a bicistronic transgene along with mCherry::H2B in order to enable quantification of the nuclear level of the ERK-substrate and avoid the need to measure it in the cytoplasm, which can be difficult for many cells inside the worm (de la Cova et al. 2017).

Another type of activity sensor is the active RHO-1 biosensor based on the Rho GTP-binding domain of ANI-1 fused to GFP. Rho can be found in a GDP-inactive or GTP-active state and the sensor was shown to concentrate on the membrane in regions where active RHO-1 was being generated by RhoGEFs in preparation for cytokinesis (Tse et al. 2012).

In a less specific approach, the fluorescent signal of a chimeric transgenic protein in muscle was used as a reporter of intracellular proteolysis (Zdinak et al. 1997). Other aspects of protein degradation visualized with transgenic FPs include ubiquitin GFP fusions which can inform on inhibition of the proteasome (Liu et al. 2011) and Ubiquitin fused with photoconvertible Dendra2

which was used to monitor rates of proteasome mediated degradation in a cell type-specific and age-dependent manner in worms (Hamer et al. 2010).

Ligand binding to the Notch receptor LIN-12 induces proteolytic cleavage and release of the intracellular domain, which enters the cell nucleus. This process has been taken advantage of to create a sensor able to report on lateral cell signaling activity (Shaffer and Greenwald 2022). The two part sensor is made of a GFP-RFP pair separated by a TEV cleavage site and a LIN-12 receptor with TEV protease fused to its intracellular domain. Activation of Notch signaling results in TEVp translocation to the nucleus and separation of GFP from RFP (Shaffer and Greenwald, 2022).

A very common type of activity reporters meant to give a visual output for the activity of transcription factors are transcriptional reporters (Okkema and Krause 2005; Boulin et al. 2006). Basically, if the DNA binding sequence of a transcription factor is present upstream of the coding sequence for an FP then when the transcription factor is active an FP will be made. High throughput projects have generated and imaged thousands of such reporters (Hunt-Newbury et al. 2007). The effect of copy number of the reporter and variability from worm to worm has been carefully studied (Mendenhall et al. 2015). One major caveat of transcriptional reporters is the temporal lag in response due to the long folding time and slow degradation of FPs, on top of transcription and translation. This caveat can partially be circumvented by using short-lived FPs. Poyurovsky et al. rendered an FP short-lived by fusing it to the RING domain of the Mdm2 E3 ubiquitin ligase, while Matilainen et al. fused the FP to an uncleavable ubiquitin segment, in both cases leading to enhanced ubiquitination and proteasomal degradation (Poyurovsky et al. 2003; Matilainen et al. 2016).

## Cellular structures and organelle dynamics

Several organelles can be specifically labeled by fusion of an FP to a canonical targeting sequence. A target sequence is a short (3–70 amino acids long) peptide chain that directs the transport of a protein to a specific structure in the cell. This way mitochondria were visualized by expressing GFP fused to a mitochondrial localization signal (Fatouros et al. 2012), peroxisomes were imaged with GFP fused to a peroxisome targeting sequence (Motley et al. 2000), and the endoplasmic reticulum (ER) was visualized by fusing GFP to the ER-resident signal peptidase SP12 (Poteryaev et al. 2005). As mentioned above, the plasma membrane can be visualized with the rat PLC1-delta plekstrin homology (PH) domain fused to GFP (Audhya et al. 2005). Alternatively, adding a myristoylation signal to any FP will target it to the plasma membrane, although it also labels membrane structures inside the cell (Chai et al. 2012). Fluorescent markers specific for the various types of vesicles in the endocytosis and exocytosis pathways are based on FP fusion with specific resident proteins in these structures, as reviewed in the worm chapter on membrane trafficking (Sato et al. 2014).

Visualization of extracellular glycans in fixed worms has been achieved by metabolic labeling of cell-surface glycans with azides, followed by click chemistry to attach a fluorophore to the azides (Laughlin and Bertozzi 2009). Direct imaging of specific heparan sulfate modification in live worms was enabled by expression of GFP-fused single chain variable fragment antibodies that recognize specifically modified forms of heparan sulfate (Attreed et al. 2012). With this technique Attreed et al. showed that while some heparan sulfate modification patterns are widely distributed in the nervous system, others appear highly cell-specific in both non-neuronal and neuronal cells (Attreed et al. 2016), and Cizeron et al. found that specific heparan sulfate

modifications stabilize excitatory and inhibitory neuromuscular junctions (Cizeron *et al.* 2021).

Lipid droplets are storage organelles important for lipid and energy homeostasis. They consist of a hydrophobic core of neutral lipids surrounded by a phospholipid monolayer and specific proteins. BODIPY, Oil Red O, and Nile Red are the commonest commercially available fluorophores used for lipid droplet staining inside live cells, including in the worm (Mosquera *et al.* 2021). The same staining methods, as well as LipidTOX, can also be used to visualize nuclear lipid droplets in intestine and germ cells (Mosquera *et al.* 2021). A fluorescent 2,1,3-benzothiadiazole (BTD)-coumarin hybrid (named BTD-Lip) developed to stain lipid droplets was shown to be superior to the BODIPY and Nile red (Mota *et al.* 2018). Feeding worms with these dyes does not lead to the staining of fat stores, but rather they accumulate in lysosome-related organelles (O'Rourke *et al.* 2009). Staining after fixation provides reproducible data, but autofluorescence and nonspecific staining of cellular structures other than fat stores can lead to errors, which has led to the development of label-free imaging of lipids using coherent anti-Stokes Raman scattering microscopy (Hellerer *et al.* 2007; Le Thuc *et al.* 2010).

The cytoskeleton is a sturdy yet dynamic structure responsible for cell shape, intracellular transport, and force generation. Since the cytoskeleton is a polymeric structure, labeling of its subunits with FPs can interfere with its polymerization. Therefore, several indirect labeling probes have been developed. In the case of actin, fusion of FPs to a variety of F-actin binding peptides, including Lifeact (Pohl and Bao 2010), Utrophin (Chia *et al.* 2012), the actin binding domain of VAB-10 (Gally *et al.* 2009), and the actin binding domain of *Drosophila* moesin (Velarde *et al.* 2007), were all used to visualize polymerized actin. It was noted in other systems that some of these probes have a preference for F-actin polymerized by specific elongation factors and therefore preferentially label subsets of the actin network (Belin *et al.* 2014). Also, when expressed at high levels these probes can affect actin dynamics (Spracklen *et al.* 2014). Evidence for such bias in *C. elegans* has not yet been reported, but it is always a good idea not to rely on a single probe and to minimize its expression when gathering information on cytoskeletal structures. Microtubule (MT) plus tip binding proteins, such as EBP-2::GFP, report the dynamics of growing MTs (Kozlowski *et al.* 2007; Tegha-Dunghu *et al.* 2014). However, they detach from depolymerizing MTs and are not present on stable MTs. To visualize the entire MT network people have labeled alpha-tubulin, beta-tubulin, and gamma-tubulin subunits (Strome *et al.* 2001; Kozlowski *et al.* 2007). Due to the redundancy of tubulin isoforms the strains expressing fluorescently tagged tubulin are viable. However, RNAi depletion of other isoforms suggests that tagged tubulin is not fully functional (RZB, unpublished data). Nevertheless, when expressed on top of other isoforms, fluorescently tagged tubulins partially incorporate into the MT lattice and illuminate its structure. The MT-binding domain of ensconsin fused to multiple copies of GFP has been used to label MTs in other organisms (Bulinski *et al.* 2001; Wühr *et al.* 2011), but as far as we know has not been used in *C. elegans*. A fluorescently tagged MT-associated protein, GFP::MAPH-1.1, was found to label noncentrosomal MTs in most if not all adult tissues (Waaaijers *et al.* 2016), though its utility as a general marker for MT has not been established. Intermediate filaments have been visualized with antibodies (Francis and Waterston 1991) and translational fusions to some of the 11 cytoplasmic isoforms, such as IFA-1a::GFP (Karabinos *et al.* 2003) and IFB-2::CFP (Hüsken *et al.* 2008).

## DNA and RNA

A number of DNA-binding fluorescent dyes, such as DAPI and Hoechst 33342, can be used to visualize DNA in the nuclei of fixed and permeabilized animals. Visualizing chromosomal DNA in live worms can be accomplished with fluorescently tagged histones [e.g. Bao *et al.* (2006)]. In order to follow specific regions of the chromosomes that are associated with unique proteins, in live or fixed samples, one can tag those proteins with FPs. This way, it is possible, for example, to visualize kinetochores (Oegema *et al.* 2001), the synaptonemal complex (Köhler *et al.* 2017), and double strand break repair sites (Alpi *et al.* 2003; Koury *et al.* 2018).

Another technique for visualizing specific DNA sequences is fluorescent *in situ* hybridization (FISH). Multiplexing dye-conjugated oligonucleotide probes it is possible in fixed samples of all developmental stages to visualize genome organization at the chromosome, 3 megabase, or 500 kb scale (Fields *et al.* 2019). Visualizing the nuclear position of a specific DNA sequence within the chromatin in live worms is possible using the lacO/lacI bacterial binding site and repressor, wherein the lacO sequence is inserted into the site of interest within the worm genome and lacI fused to an FP is expressed in the desired cells (Carmi *et al.* 1998). This method is elaborated upon in the Wormbook chapter on chromatin analysis (Feinberg *et al.* 2008). The LacO/LacI system can be combined with a nanobody against histone H4 Lys20 mono-methylation (H4K20me1) to visualize locus-specific H4K20me1 modifications in living worms (Shinkai *et al.* 2018). In mammalian cells, fluorescently tagged catalytically inactive Cas9 endonucleases were used to label specific DNA sequences based on the cognate single-guide RNAs (Deng *et al.* 2015; Ma *et al.* 2015), and this method should, in theory, work in *C. elegans* as well.

Single molecule FISH (smFISH) of fluorescent oligonucleotide probes on fixed samples enabled to study intracellular mRNA localization at single mRNA level in embryos and larva (Raj *et al.* 2008; Ji and van Oudenaarden 2012). Visualizing the dynamics of mRNA transcripts in live worms has been achieved using the MS2/MCP system or the PP7/PCP system, both based on specific protein-mRNA interactions (Lee *et al.* 2019; Li *et al.* 2021). Lee *et al.* (2019) used the MS2 system to follow bursts of *sygl-1* transcription downstream of Notch signaling. Li *et al.* (2021) generated a collection of strains for visualizing mRNAs encoding apical, basolateral, and junctional proteins in *C. elegans* epithelia, using the PP7 system. RNA condensates have been visualized by tagging the intrinsically disordered proteins that phase separate together with the RNA. For example, fluorescently tagged PGL-1 is used to mark P-granules, tagged WAGO-4 and ZNFX-1 to mark Z-granules, and MUT-16 labels the mutator complex (Phillips *et al.* 2012; Wang *et al.* 2014; Wan *et al.* 2018; Lev *et al.* 2019).

## Cytoplasmic ions and second messengers

Calcium ions serve as important secondary messengers in neurons and muscle cells. During a signaling event the concentration of calcium usually rises sharply before dropping quickly (Chung *et al.* 2013; Kovacevic *et al.* 2013). It is possible to visualize the sudden increase in concentration of calcium ions with a fluorescent probe that changes its fluorescent properties upon binding calcium. One such probe is GCaMP, a fusion of GFP with calmodulin and M13, a peptide from myosin light chain kinase that binds calmodulin. GFP is circularly permuted so that the N- and C-termini are fused and calmodulin and the M13 peptide are fused to new termini in the middle of the protein. GCaMP was engineered so that its fluorescence is very low in the absence of calcium. A conformational change in the protein following the calcium-



dependent binding of M13 to calmodulin leads to a many fold increase in the fluorescence intensity of GFP. Calcium sensors have been particularly beneficial for neurobiology, enabling researchers to detect the activity of single neurons, and, when combined with optogenetic tools for activating neurons, facilitated the mapping of neuronal circuits (Guo et al. 2009; Tian et al. 2009; Emmons et al. 2021). Remarkably, calcium imaging of neuronal activity has been achieved even in freely moving worms (Nguyen et al. 2016; Venkatachalam et al. 2016; Gengyo-Ando et al. 2017). Calcium signaling also regulates muscle contraction and was monitored using GCaMP in the body muscle during the wake-sleep cycle (Schwarz et al. 2012) and in the spermatheca during embryo transit (Bouffard et al. 2019). Mutagenesis of GCaMP resulted in more sensitive sensors (Devkota et al. 2021) and additional colors of genetically encoded calcium indicators, including red (R-GECO1) and blue (Zhao et al. 2011).

Acidity is a chemical property of the cytoplasm or intracellular fluid that can be visualized. Expression of the pH-sensitive GFP variant pHluorin in various tissues has facilitated the visualization of intracellular acidification following mitochondria fragmentation (Johnson and Nehrke 2010). A pH-responsive dye, KR35, was used to monitor pH in the intestine of *C. elegans* (Bender et al. 2013). KR35 is activated by acid in a range that is physiologically relevant to the *C. elegans* intestine.

cGMP is a second messenger with an important role in regulating ion channels. In the worm it is implicated in the function of many sensory neurons. A FRET-based sensor, in which a cGMP-binding domain is sandwiched between CFP and YFP, was used to visualize spatiotemporal cGMP dynamics in AWC neurons after odor exposure (Shidara et al. 2017). A GFP-based cGMP sensor was also adapted from mammalian cells for use in worms and was shown to provide a sensitive readout of cGMP levels in body wall muscles (Woldemariam et al. 2019). This sensor contains 2 in-tandem PKG cGMP-binding domains attached to the N-terminus of a circularly permuted EGFP. Similar to GCaMP, the fluorescence of the sensor is low in the absence of cGMP and high when cGMP binds the PKG domains.

Following the same principle, FRET sensors were developed for ATP (Tsuyama et al. 2013) and for inorganic phosphate (Bender et al. 2013).

## Apoptosis

The first worm Nobel prize, awarded in 2002, was for discoveries on the genetic regulation of organ development and programmed cell death (apoptosis). The simplest way to visualize cell death, employed by Brenner, Sulston, and Horvitz in their Nobel-winning work is by DIC microscopy, taking advantage of the unique button-like shape of cell corpses (Sulston and Horvitz 1977; Sulston et al. 1983). It is also possible to detect apoptotic cells in live worms by staining them with acridine orange or SYTO 12 vital dyes, which stain nucleic acids specifically within the dying cells (Lant and Derry 2014). An indirect method to visualize dead cells is with CED-1::GFP, which is expressed in the neighboring cells that engulf the dying cells (Zhou et al. 2001). CED-1 is a transmembrane receptor that clusters around cell corpses. This last method is very sensitive but does not work in engulfment defective mutants.

## Mechanical force

Many proteins in the cell, most notably those associated with cell adhesion and the cytoskeleton as well as extracellular proteins, experience varying levels of mechanical tension during development and throughout the worm's life. Such tension arises when

the protein is anchored at both ends and is being stretched. Two FRET-based sensors have been deployed in worms to visualize such tension and qualitatively assess how it is affected by different treatments. The first tension sensor (stFRET) consisted of 2 FPs, Cerulean and Venus, joined by a 5-nm protein helix and it was inserted into collagen-19 (Meng et al. 2011). Stretching forces, which were determined in vitro to be 5–7 pN, would stretch the alpha helix, increase the distance between the FP and reduce the FRET signal. In this way, it was shown that the collagen in the cuticle is constitutively stretched. A second tension sensor module (TSMOD) introduced into beta-spectrin in worms contained mTFP1 (TFP: teal FP) and Venus as the FPs and used a 40-amino acid sequence derived from spider silk protein as the flexible linker (Fig. 2f). Using this probe it was demonstrated that spectrin is held under constitutive tension in touch receptor neurons, which contributes to touch sensation (Krieg et al. 2014).

## Microscopy

In the past decade advances in sensor, optical, and system design have yielded steady improvements in imaging resolution and speed. This has produced a dizzying array of options for the biologist and selecting an optimal instrument to buy or use can be a confusing process. These advanced microscopy modalities have been applied to a range of specific biological questions in the worm, some prominent examples are listed in Table 2. In this section, we will briefly review the technical considerations inherent to a range of cell biological and developmental imaging experiments as they pertain to instrument selection and provide a snapshot of relevant advances in imaging technology that may be leveraged. While many variations of each class of microscope exist in the marketplace today and many more continue to be introduced, Fig. 3 provides a simplified illustration of the key operational principle of 4 prominent classes of fluorescence microscopes especially well-suited to live imaging in *C. elegans*. It is worth noting that these modalities are not mutually exclusive and can be integrated into single multifunctional instruments that may be a cost-effective, albeit more complex solution for the core facility or technically savvy research group.

## Localization and colocalization

In the context of selecting an instrument to use in measuring molecular localization or colocalization, it is useful to start with 3 basic questions:

- How bright is the labeled protein?
- What sub-cellular structures does the protein appear to localize to?
- Is localization expected to be highly dynamic?

For these and many other types of imaging experiments, it makes sense to apply a pyramidal approach by beginning with simple compound fluorescence microscopes and sequentially moving to more complicated instruments based on the observed characteristics of a particular tag and the strengths and weaknesses of the microscope modalities available (Fig. 4).

While protein localization can be measured by a wide variety of microscopy modalities, given the considerations listed above, colocalization imposes some additional technical considerations. Most methods of colocalization involve the use of multiple FPs with differing excitation and emission spectra. For live samples where proteins may be freely diffusing, or where colocalization may be a dynamic equilibrium process, rapidly acquiring images

**Table 2.** Biological findings in *C. elegans* employing a range of advanced microscopy modalities.

Biological observation	Microscopy modality	Reference
Automated lineage tracing	Laser scanning confocal Spinning disk confocal Lightsheet	Bao et al. (2006) Moore et al. (2013) Duncan et al. (2019)
Retrograde zippering in neuritis	Lightsheet	Sengupta et al. (2021)
Organization of p-granules	SIM-mode lattice lightsheet	Wang et al. (2014)
Structure of muscle attachment	SIM	Qadota et al. (2017)
Organization of $\beta$ spectrin in neuritis	SIM STED	He et al. (2016) Krieg et al. (2017)
Clustering of glutamate receptors	PALM	Vangindertael et al. (2015)
Organization of meiotic chromosomal axes	PALM and STORM	Köhler et al. (2017)

in 2 or more colors can be challenging without multiple detectors or color splitters for simultaneous multicolor imaging. In these cases, correcting for chromatic aberrations that may be integral to the imaging optics and for alignment errors between multiple sensors is necessary to produce robust measurements. Multicolor bead standards are a useful tool in assessing these issues and can be used in conjunction with freely available software (Preibisch et al. 2010) to computationally correct for simpler aberrations.

### Dynamic measurements

The greatest advantage of live sample microscopy is the ability to follow dynamic biological processes over long timescales and relate molecular events to their cellular and organismal consequences. Increasingly sensitive light sensors and new microscopy modalities have resulted in huge advances in our ability to capture dynamics processes across the entire worm with subcellular spatial and sub-second temporal resolution. A tradeoff still exists between spatial resolution, temporal resolution, and sensitivity, however, requiring some careful consideration of the desired spatial and temporal scales over which a phenomenon is to be observed. Modern wide-field, spinning disk confocal, pixel reassignment SIM, and lightsheet microscopes are now limited in acquisition rates almost entirely by their cameras. Commonly used sCMOS cameras can achieve full frame imaging at 100 frames per second (FPS) or more, with higher rates possible for subregions of the sensor. More exotic intensified CMOS cameras have also been demonstrated recently, which can produce usable images with submillisecond exposure times for bright samples (Voleti et al. 2019).

Important for optimizing long-term imaging experiments is the balance between image brightness and resolution against the potential confounding factor of biological perturbation from excitation light. Photobleaching fusion proteins can result in the direct inactivation of the tagged protein to the extent that it has been employed as a means of optogenetic perturbation (Ou et al. 2010). For embryonic and larval experiments, a useful empirical metric for photodamage is developmental progression: imaging conditions that compromise animal viability enough to block or significantly delay developmental progression should be avoided.

### Quantitative microscopy

Making robust, repeatable measurements of physical quantities by light microscopy requires careful preparation and the integration of robust technical controls into the experiment. Intensity standards have long been used in the calibration of flow cytometers and can be equally valuable tools as spike-in or periodic controls when intensity measurements across multiple days or samples need to be made in a repeatable fashion.

Most image sensors are calibrated to produce a linear output for increasing incident light. Multiplicative sensors such as

photomultiplier tubes (PMT), avalanche photodiodes (APD), and electron-multiplying CCDs (EM-CCDs) can exhibit some variability in their signal amplification and introduce noise into signal quantification. This noise can be measured using constant signal standards (such as uniform fields of dye solution or intensity-calibrated bead dispersions) when a high degree of linearity and precision in signal measurement is required.

For quantitative microscopy to be repeatable and reproducible, recording and sharing careful documentation of imaging parameters and performing day-of-control measurements is a critical yet underutilized step. Recent works have detailed best-practices in quantitative microscopy for different instrument modalities, as well as for reporting methods in imaging and image analysis, which should be required reading for the imaging scientist in-training (Waters 2009; Jonkman et al. 2020).

### Selecting objectives

Depending on the nature of the experiment and manner in which the worm must be mounted, selecting an objective with the appropriate magnification, numerical aperture, and immersion medium can produce brighter, higher resolution images with lower excitation powers or shorter camera exposures.

Dry, or “air-immersion” objectives are best suited for routine inspection and for screening worms on plates. For higher resolution and more sensitive imaging experiments, use of a liquid immersion media between the objective and coverslip helps increase the angle of collection for light and reduce aberrations caused by the drastic change in refractive index between glass ( $n = 1.517$ ) and air ( $n = 1.0$ ). The most common liquid immersion media include water ( $n = 1.333$ ), silicone oil ( $n = 1.406$ ), glycerol ( $n = 1.45$  for 80% glycerol in water), and immersion oil ( $n = 1.517$ ). Higher refractive index immersion media enable light collection over a wider angle and thus a higher maximum numerical aperture, typically a maximum of 1.5 NA for standard immersion oil. Exotic immersion media with refractive indices greater than that of standard oil enable even higher numerical apertures, but these are typically limited to collecting signal close to the coverslip surface such as by TIRF (TIRF: total internal reflection fluorescence) microscopy and are prone to severe aberrations when used to image thicker samples.

An important consideration for minimizing aberrations while imaging inside of worm tissue is the degree of mismatch between the refractive index of the immersion media and that of the tissue. Tomographic phase microscopy of a *C. elegans* adult has previously measured a range of refractive indices for worm tissue from 1.36 up to 1.38 (Choi et al. 2007). In this region, between the refractive indices of water and silicone oil, silicone oil has notable advantages for confocal microscopy due to the higher numerical aperture (a maximum of 1.35 vs 1.27 for water). For imaging in



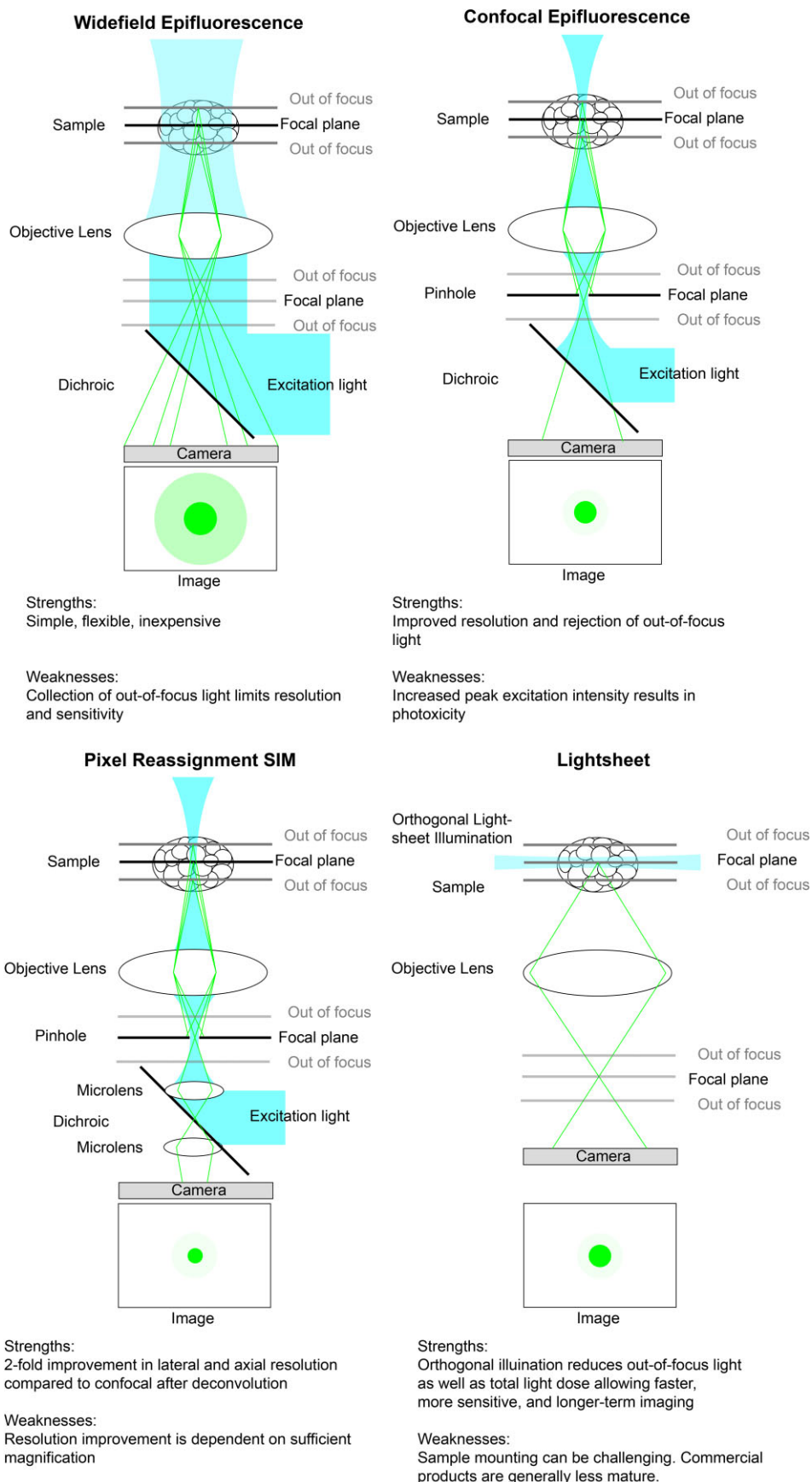


**Fig. 3.** Simplified illustrations of the operating principles of widefield, confocal, pixel reassignment SIM, and lightsheet microscopes with a summary of their key strengths and weaknesses.

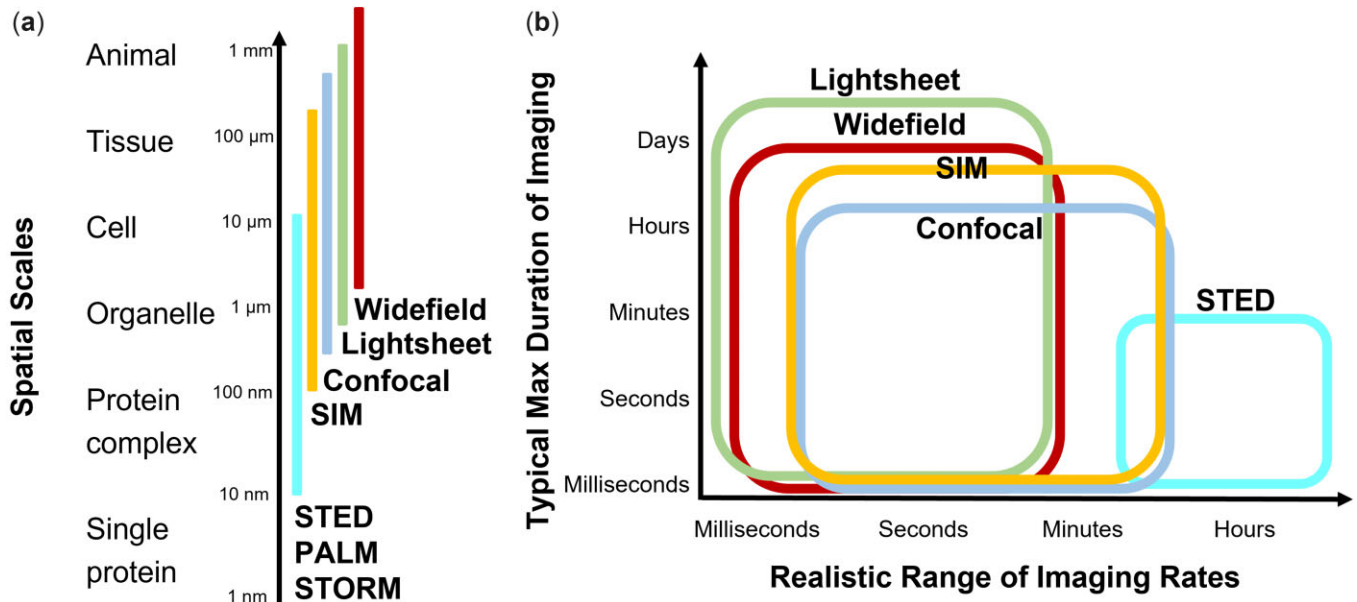


**Fig. 4.** a) Accessible spatial scales across common microscopy modalities. Resolution and field-of-view limits within classes of microscopes vary based on several factors including objective selection, sample mounting, and detector choice. b) Maximum imaging rates (the number of frames that can practically be acquired per unit time) and the duration over which imaging can occur (before toxicity or bleaching typically become prohibitive) vary wildly and are also highly sample dependent.

surface tissues, the hypoderm and muscle especially, conventional immersion oil can be advantageous due to simpler operation and higher numerical apertures. For cases where the worm cannot be compressed against the glass surface to minimize the invasion of mounting buffers between the sample and the microscope, replacing a fraction of the water in the buffer with iodixanol can be used to match the refractive index of the mounting buffer to that of the immersion media and improve image quality (Boothe et al. 2017).

Microscope objective performance can vary widely between offerings from different manufacturers, and between immersion media. While some degree of performance can be predicted from specifications such as magnification, numerical aperture, and working distance, significantly more care must be taken for super resolution microscopy. In some cases, subtle aberrations caused by defects in materials and manufacturing may only be detectable by the empirical measurement of the microscope's point spread function when fitted with a new objective (Theer et al. 2014).

### Common modalities for fluorescence microscopy

The past decade has seen an explosion in the availability of previously exotic imaging modalities or unusual flavors of basic classes of microscopes. In this section, we will provide a big-picture overview of these approaches (Fig. 3), review typical use cases for each in the context of *C. elegans* biology, and refer the reader to more detailed discussions of the technical details of the relevant methodologies.

#### Widefield imaging

While the epifluorescence microscope is now more than century old, it remains one of the most flexible and accessible platforms for routine and advanced fluorescence microscopy techniques alike. Advances in cameras, light sources, and computational approaches to postprocessing have kept the venerable widefield microscope more than relevant even in the age of structured illumination and light sheet microscopy.

In the context of *C. elegans*, where labeled tissues and structures are often distributed in 3D, widefield microscopy is essentially a tradeoff between light throughput and the ability to separate signal within the focal plane from out-of-focus signal and autofluorescence. Iterative deconvolution algorithms, now efficient enough to run in near real-time thanks to parallel computing on graphics cards allow for the algorithmic removal of out-of-focus light (Swedlow 2013). Every major microscope vendor now offers integration with deconvolution algorithms with their microscope control software, and several major vendors and open-source projects (Sage et al. 2017) offer advanced stand-alone software for deconvolving images postacquisition. For sparse and bright labels, deconvolution microscopy can be competitive with confocal microscopy while being faster and gentler on live samples.

Compared with brightfield imaging, 3D fluorescence microscopy in live samples is often limited by phototoxicity and photobleaching from fluorescence excitation. The toxicity induced by the intense illumination required for fluorescence excitation must be balanced against the frequency with which a sample can be imaged. While only the fluorescence light emitted from the focal plane of the objective is informative to collect, most microscopy modalities continuously bathe the entire depth of the sample in excitation light.

#### Confocal microscopy

The history of the laser scanning confocal microscope (LSCM) is intimately tied to the history of *C. elegans* biology by the seminal contributions of John White and Brad Amos to the development of beam scanning as a mode of confocal imaging (White et al. 1987). LSCM operates by projecting a single spot of laser illumination onto the sample and filtering collected fluorescence through a pinhole at conjugate plane. The size of the pinhole blocks most of the out-of-focus light collected by the objective since light from different depths in the sample will converge to a focus before or after the pinhole. The microscope then scans this spot across the sample, allowing simple detectors to be used to

measure fluorescence intensity at each scan position to build up an image. Since each pixel in the image is acquired sequentially, the amount of time for which each pixel can be exposed must be extremely short to enable image acquisition within practical timescales. To compensate for this, high peak excitation intensities are used to maximize the number of photons that can be collected for each pixel. Using sensors with multiplicative gain like PMTs and APD allows for the amplification of the extremely small amounts of light collected to produce an electrical signal that can be easily measured. Since small numbers of photons are collected per pixel, LSCM images are highly prone to shot noise, also known as photon counting noise, which is typically dealt with by averaging multiple scans over the field of view, further exacerbating the speed limitations imposed by sequential scanning. While modern LSCM's can achieve scan rates in the 10–20 FPS range to cover a full field of view, practical constraints such as the brightness of the sample and the need to average multiple frames to reduce shot noise mean that most imaging experiments will achieve significantly lower frame rates.

Spinning disk confocal (SDC) and multipoint scanning confocal (MPSC) microscopy mitigates the primary disadvantage of LSCM by parallelizing the scanning process. Since multiple pinholes are within the field of view at any given moment, the entire image can be collected significantly faster than with LSCM while also dramatically increasing the effective dwell time, or time spent exciting and collecting fluorescence from each point in the sample. This increases the number of photons that can be collected from the sample in a single exposure, and thus allows for significantly lower peak excitation intensities and thus less photodamage from the imaging process. Pinhole crosstalk, when light collected through adjacent pinholes overlaps on the sensor, can reduce spatial resolution in these systems in especially thick samples or when the pinhole spacing is optimized for a higher magnification than is used, however this is generally not a major problem for imaging in worm tissue, except in cases where exceptionally bright sources of fluorescence are present in the sample. Modern SDC and MPSC's can acquire images at rates limited entirely by the cameras used, more than 100 FPS in many cases. For especially dim and light-sensitive samples, these rates are not often practically achievable, but 10 FPS or more can easily be achieved even in the most demanding applications like the minute-by-minute imaging used for tracing cell lineages in the *C. elegans* embryo (Santella et al. 2010).

### Structured illumination microscopy

Structured illumination microscopy (SIM) relies on extra information content present in images acquired when nonuniform illumination patterns are applied to a sample to improve lateral and axial resolution compared with homogeneous illumination. The most common form of this approach applies illumination patterns of varying phase and reconstructs an image with improved lateral and axial resolution. While the underlying mechanism is the same, this class of SIM is broadly categorized as either 3D-SIM, when the goal is to reject out-of-focus light and provide improved optical sectioning, or super-resolution/SR-SIM, when the goal is to reconstruct an image with resolution exceeding the diffraction limit of light. In both cases, a wide variety of commercial systems are available that automate the image acquisition and postprocessing tasks. While SIM can be faster and gentler on samples than LSCM, it is more susceptible to aberrations in thick samples where the illumination pattern can become corrupted by passing through the sample. This limit must be determined empirically for each SIM implementation and

sample due to differing depth-dependent performance between objectives and variability in the scattering and refractive properties of different tissues. Compared with multipoint confocal microscopy, the maximum achievable frame rates are significantly slower due to the need to acquire multiple images with different illumination patterns to reconstruct a single final image.

A newer class of SIM has recently become widely available in commercial products, termed pixel reassignment SIM. Pixel reassignment SIM relies on multipixel detectors (cameras or multipixel PMT arrays) to collect an image of the emitted light after filtering through a pinhole. Since some of the pixels are shifted laterally relative to the center of the pinhole, fringes of the diffraction pattern are collected that contain higher spatial frequency information. Reassigning the signal collected at these points can achieve a factor of  $\sqrt{2}$  (~40%) improvement in resolution compared with confocal microscopy. The reassignment can be done digitally, in the case of single point scanning implementations such as the Zeiss Airyscan, or optically, in the case of multipoint scanning implementations such as the Visitech iSIM (York et al. 2013) or Yokogawa SoRa (Super resolution via Optical Re-assignment). Both digital and optical reassignment maintain high-frequency (and thus high resolution) information in the final image, although multipoint implementations offer a significant advantage in speed just as when comparing LSCM with MPSC microscopy. These approaches can typically match the image acquisition rate of the corresponding confocal modality with a slight increase in light dose. Since the patterned illumination in this case is simply a single focused laser spot or array of spots and the emitted light is filtered by imaging onto a small sensor (e.g. Airyscan) or by a pinhole array or disk at a conjugate plane (e.g. iSIM, SoRa), pixel reassignment SIM performs better in thick samples compared with 3D or SR-SIM (Wu and Shroff 2018).

### Light sheet fluorescence microscopy

Light sheet fluorescence microscopy (LSFM), also referred to as single plane illumination microscopy (SPIM), improves on conventional fluorescence microscopy by introducing excitation illumination in a single “sheet” aligned parallel to the imaging plane. This allows high quality optical sectioning to be achieved without a confocal pinhole or nonlinear postprocessing as in 3D-SIM. Since only the section of the sample being imaged is illuminated, photodamage is also significantly reduced, allowing image acquisition to occur faster, more frequently, or for longer without affecting sample viability.

LSFM employs a wide range of approaches for generating excitation sheets of various geometries, collecting emitted light, scanning axially through a sample, and reconstructing images. An exhaustive treatment of these implementations is beyond the scope of this chapter but can be found in the literature (Power and Huisken 2017). Imaging in *C. elegans* embryos, larvae, and adults imposes some unique constraints on sample mounting and imaging that somewhat restrict the approaches to LSFM that are best suited for worm imaging.

Due to the complex instrument geometries used to deliver the light sheet to the sample and collect fluorescence, proper sample mounting is even more critical. Instruments employing dipping objectives where the sample chamber must be flooded with buffer are best suited for imaging embryos, although larvae and adults can be made accessible by gel-embedding. Instruments capable of imaging through a glass coverslip are compatible with more sample mounting and immobilization strategies but are typically limited to a single view of the sample.



Multiview LSFM takes advantage of the most common strategy for generating light sheet illumination, using 2 perpendicular objectives to project the light sheet and collect the image, to overcome the anisotropic resolution of conventional microscopes and depth-dependent light loss due to aberrations and scattering when imaging thick samples. In its simplest form, 2 perpendicular views of the sample are acquired and jointly deconvolved to produce images with isotropic resolution. This computational strategy is extremely efficient if multiple views can be acquired faster than any object being imaged can move appreciably, since a 2-fold increase in light dose and imaging time produces a 6-fold improvement in axial sampling (Wu *et al.* 2013).

### Super-resolution techniques

Super-resolution microscopy via SIM is currently the most accessible for imaging live samples; however, there are other methods that offer complementary capabilities and finer spatial resolution. Classical localization techniques, where either stochastic processes or photoswitchable fluorophores are employed to achieve single molecule fluorescence detection, have been successfully applied in *C. elegans*. These methods can achieve spatial resolutions on the order of 10's of nm, but typically only in fixed samples and with minimal optical aberrations (Vangindertael *et al.* 2015; He *et al.* 2016; Köhler *et al.* 2017). While these approaches require samples to be fixed, other super-resolution techniques including stimulated emission depletion (STED) (Rankin *et al.* 2011), and super-resolution optical fluctuation imaging (Kurshan *et al.* 2018) have also been employed in live worms. In fixed samples, the optimization of expansion microscopy (ExM) for *C. elegans* now makes it possible to achieve super-resolution imaging of protein localization and cellular anatomy with standard widefield or confocal microscopes, since the resolution improvement comes from embedding the sample in a hydrogel and causing it to swell, which physically moves individual fluorophores or sample epitopes further apart from one another (Yu *et al.* 2020). Lambert and Waters provide a sober view on the current limitations and compromises that must be made when designing super resolution experiments (Lambert and Waters 2017).

## Image analysis

Both automated and manual image analysis have made great strides in the past decade owing to an explosion in the

computational power available in inexpensive desktop and even laptop computers. Parallelized processing using graphics cards intended for gaming now makes it possible to execute analysis pipelines on a personal computer that once required dedicated high-performance hardware. Along with these advances, modern programming languages such as Python have made it possible for even novice programmers to build sophisticated and powerful customized applications quickly and easily for processing images. In this section, we will discuss some widely used open source and commercial software packages for image analysis.

### Common tasks in image analysis

Despite the aforementioned advances, image analysis remains a major practical bottleneck. Overcoming this requires understanding some of the capabilities and challenges of automation: there are simply some tasks that computers excel at and others that they struggle with. Here we discuss three broad categories: image processing, image analysis, and visualization.

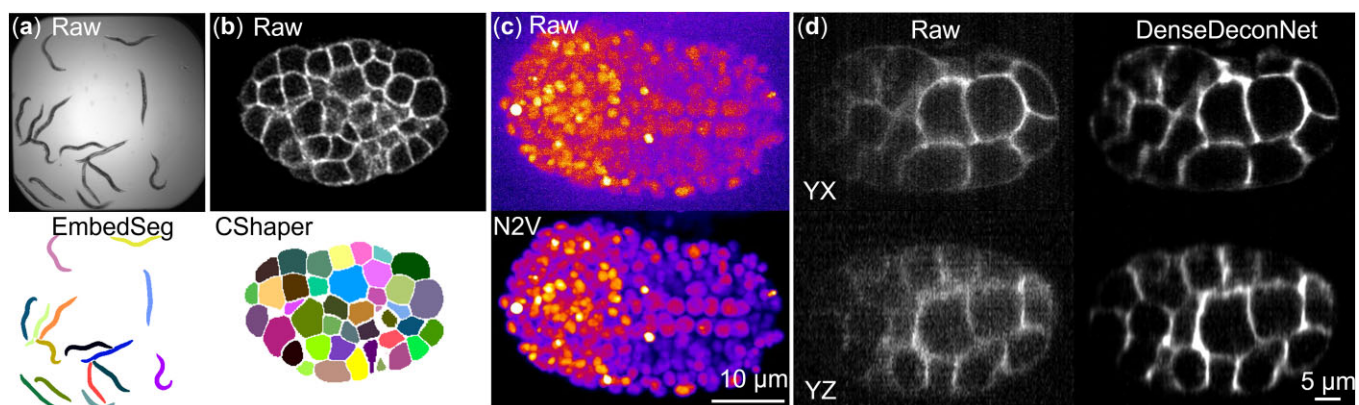
#### Image processing

Image processing generally refers to manipulations applied to images to either mitigate undesirable features of images or enhance specific features in images to aid in visualization and downstream analysis. Typical image processing tasks can include filters to reduce background and mitigate noise, deconvolution to improve resolution, or feature enhancement to emphasize specific features in images such as edges, lines, or blobs. Selecting the right image processing strategy can dramatically improve the performance of downstream analysis, but care must be taken that the processing itself does not introduce new artifacts into the images. Manually inspecting the results, performing detailed control experiments, and fully documenting and sharing processing steps and scripts can help to prevent this issue.

#### Image analysis

Image analysis can largely be broken down into some combination of 4 tasks: stitching, segmentation, tracking, and measurement.

Image stitching is required when a specimen is too large to fit into a single field of view, for example, when an entire worm is imaged at high magnification. Multiple images with some overlap can be aligned and fused to form a single image using Fiji stitching tool or BigStitcher (Hörl *et al.* 2019). Segmentation is the process by which objects in an image are identified and separated



**Fig. 5.** a) Segmentation of adult worms in brightfield imaging via EmbedSeg (Lalit *et al.* 2021) Image Credit: Manan Lalit. b) Segmentation of membrane-targeted fluorescence images of *C. elegans* embryos using CShaper (Cao *et al.* 2020) Image Credit: Manan Lalit. c) Denoising H2B::mCherry expressing embryos without reference training data using Noise2Void (Krull *et al.* 2019) Image Credit: Pavak Shah. d) Inference of lightsheet images with isotropic resolution from a single view using DenseDeconNet (Guo *et al.* 2020) Image Credit: Min Guo.

from each other and from the background of an image (Fig. 5a and b). For example, objects to be segmented could be nuclei, cell–cell junctions, mitochondria, chromosomes, or MTs. The simplest possible approaches to segmentation, such as intensity thresholding, fail when cells or structures in an image are near or touching one another and when there is high or uneven background in the image (for example, due to autofluorescence). Increasingly sophisticated approaches, such as those based on the watershed transform or kernel filters that try to pick out objects of a specific shape or size, can require a fair amount of optimization. Most general-purpose image analysis software such as those listed below implement many such approaches that can be iteratively tuned and then applied to large sets of images automatically. A key challenge here is the question of generalizability, since a particular pipeline with preselected parameters is unlikely to produce accurate results on data generated using a different microscope, at a different magnification, or with different labels, without reoptimization.

Tracking objects through timelapse image data is a major challenge for many live imaging experiments. There are generally 2 classes of tracking approaches: object tracking and pixel tracking. In object tracking, a dataset is first segmented and individual objects are linked across successive timepoints based on metrics such as distance, overlap, and similarity. This is by far the most common approach to tracking cells, as well as vesicles, in live imaging experiments. Pixel-based tracking does not depend on prior segmentations and instead attempts to estimate displacements in an image on a per-pixel basis, typically by optimizing some physical model over measures of pixel-wise changes in intensity between successive frames. This approach tends to produce good results when large numbers of objects are present and their movement between successive frames is quite small. For example, it was used to track cytoplasmic streaming in the rachis (Priti et al. 2018) and actin cortical dynamics in the zygote (Ding et al. 2017).

Measurement tools found in image analysis software such as Fiji (Schindelin et al. 2012) can be used to quantify various parameters of the segmented image (e.g. fluorescence intensity, area, length, and circularity of segmented structures), or of the tracked objects (e.g. number of particles, speed, length of track), or of an entire image. When fluorescence intensity is being quantified it is paramount that all images, including controls, be acquired under the same imaging conditions (same microscope, laser power, exposure time, etc.).

### Visualization

Displaying multidimensional images in a clear manner can be a significant challenge but a wide range of new software packages make it easier to render and display complex datasets. General-purpose software such as ImageJ (Collins 2007) and Fiji (Schindelin et al. 2012) offer slice-viewers that can render 3D datasets on a slice-by-slice basis, support false coloring of multidimensional data, and include a wide range of built-in tools for generating projections and mosaics of 3D data, several tools are now available that support a broader range of visualization features. BigDataViewer (Pietzsch et al. 2015) is available as a Fiji plugin and supports the visualization of large-scale, multichannel, and multiview images. While it was developed primarily to support the visualization of light sheet microscopy data that can be terabytes in size, it is an excellent tool for rendering any large multidimensional image set. ClearVolume (Royer et al. 2015) is a volume renderer that is also available as a Fiji plugin, supporting the display of large multidimensional datasets. In addition to supporting image analysis routines, Napari (2019) also supports

interactive and script-based image visualizations and animations. It is important to note that single channel imaging data are best presented in figures in grayscale or monochrome (or inverse monochrome) rather than in pseudocolor because the human eye is far better at detecting changes in grayscale than in color (Jambor et al. 2021).

The invariance of *C. elegans* anatomy has led to the development of several digital models of the worm to which image data can be compared or that are themselves derived from worm imaging experiments. WormGUIDES (Santella et al. 2015) provides a graphical representation of *C. elegans* embryogenesis, rendering the 3D positions of every cell in the embryo starting from before the 4-cell stage and currently leading up to the point at which twitching begins. In addition to displaying cell positions, WormGUIDES can also render complex morphologies and serves as a spatial index to the embryo, allowing queries to be made against WormBase for additional information such as gene expression.

### Generalized tools

Most commercial software packages for image analysis readily integrate a wide range of processing pipelines for basic tasks that can be strung together to suit most measurement tasks. Stand-alone software such as Imaris (Oxford Instruments) and Aivia (Leica Microsystems) and integrated solutions by major microscope vendors including CellSens (Olympus), NIS-Elements (Nikon), and ZEN (Zeiss), are readily available for individual labs to purchase or often through local imaging core facilities. All these tools are capable of basic segmentation and tracking tasks, however, some have recently implemented novel capabilities, such as support for lineage tracing in Imaris and for machine learning-based segmentation and processing in Aivia. A wide range of open-source tools are also available, although the features available in each change frequently as new plugins and improvements are published. GUI-based tools such as Icy (de Chaumont et al. 2012), CellProfiler (McQuin et al. 2018), and Fiji (Schindelin et al. 2012) are broadly used and support a range of common and specialized image analysis tasks. CellProfiler also has a dedicated worm toolbox that enable the segmentation, scoring, and straightening of whole worm images (Wählby et al. 2012). New platforms under active development, such as Napari (2019), offer increasingly powerful support for integrating flexible image visualizations with advanced image processing and analysis routines.

### Specialized tools

#### Colocalization

A wide range of metrics exist for the quantification of colocalization and have been thoroughly described in the literature. Many of these metrics have been implemented as ImageJ plugins, allowing them to be performed quickly and easily (<https://imagej.net/imagining/colocalization-analysis>).

#### Embryonic cell lineage tracing

For *C. elegans* lineage analysis, only 2 software packages under active development support cell lineage tracing in the embryo: Simi BioCell (Schnabel et al. 1997) and StarryNite (Santella et al. 2010, 2014)/AceTree (Boyle et al. 2006; Katzman et al. 2018). Simi BioCell enables lineage tracing through a manual interface where the user can follow individual cells through development by clicking on their location through subsequent frames and provides 3D and lineage tree visualizations for rendering the results. StarryNite and AceTree are used together for tracking and curation, respectively, and are open-source software built from contributions by several labs. StarryNite is a MATLAB-based

application that is optimized for detecting and tracking fluorescently labeled cell nuclei. Its companion software, AceTree, provides a graphical interface for visualizing the tracking performed by StarryNite and for correcting errors and applying canonical names to cells based on their lineage. An extension to StarryNite and AceTree, called ShootingStar was also developed to enable real-time lineage tracing in developing embryos in order to automate optical perturbations such as laser ablation and photoconversion-based labeling (Shah et al. 2017). Semiautomated lineage tracing in fluorescence imaging was also previously achieved via complementary approaches (Carranza et al. 2011; Giurumescu et al. 2012; Mace et al. 2013). An extension to lineage tracing is the automated extraction of cell shapes from the developing embryo. The robust segmentation of fluorescently labeled membrane images is a challenging problem exacerbated by the anisotropic sampling of confocal microscopes. Previous efforts have produced tools that perform reliably in early-stage embryos (Azuma and Onami 2017), and more recent advances in machine learning have enabled significant progress in this field (see *Machine learning*).

Some attempts have also been made to automate cell lineage tracing in twitching embryos and postembryonic worms. While the image analysis problem is similar, long-term imaging and stabilization of images in mobile life stages poses notable challenges. Untwisting the *C. elegans* embryo provides a direct route to the stabilization of post-twitching embryos to enable cell tracking (Christensen et al. 2015). Intermittent microfluidic immobilization has also enabled long-term imaging of postembryonic development, such as in the vulval lineage (Keil et al. 2017; Berger et al. 2018).

## Machine learning

Machine learning in the form of deep neural networks has revolutionized many aspects of image processing and analysis. Many such tools require the user to train models using their own data, but a few general tools now exist. While implementing these pipelines in one's own laboratory may seem daunting, more user-friendly resources such as DeepImageJ and Ilastik are now available (Berg et al. 2019; Gómez-de-Mariscal et al. 2021).

Neural network-based approaches to image denoising have notable advantages for image segmentation and tracking tasks where the goal of the processing is to produce reconstructed images with higher contrast for further analysis. Supervised (where example high contrast images are paired with noisy low contrast images) approaches such as CARE (Weigert et al. 2018) and unsupervised (where only a noisy low contrast image is provided) approaches such as Noise2Void (Fig. 5c; Prakash et al. 2020) to neural network-based denoising have shown significant promise. Specific imaging modalities that enable deep learning approaches allow for the acceleration of classical processing algorithms such as deconvolution but can also speed up imaging by reconstructing high resolution images from incomplete data as in multiview lightsheet microscopy by DenseDeconNet (Fig. 5d; Guo et al. 2020). It should be emphasized that images processed by nonlinear methods such as deep neural networks should not be treated as quantitative as far as image intensity is concerned. The improvement in the signal to noise ratio can be useful for segmentation and tracking tasks, but any quantification should be performed on minimally processed data.

Neural network-based segmentation strategies have similarly progressed by leaps and bounds. Training these networks remains a major bottleneck as no fully plug-and-play solutions compatible with 3D datasets have yet been published, although

progress in general models for cell segmentation in 2D cell culture and tissue section samples is encouraging. For users with a large enough use-case to warrant investing the effort required to train such networks, a range of tools exist which now enable 3D segmentation of blob-like structures like nuclei (StarDist; Weigert et al. 2020) or more complex structures such as overlapping worms in brightfield images [EmbedSeg, Fig. 5a (Lalit et al. 2021)] or cell boundaries in fluorescently labeled embryos [CShaper, Fig. 5b; Cao et al. (2020)]. An application that is bound to benefit from these deep learning methods is the automated reconstruction of whole-embryo cell lineages (Malin-Mayor et al. 2021).

## Outlook

Going forward, we believe that imaging will continue to be tightly knit with worm biology. The application of cutting-edge imaging techniques will open new biology to be investigated in the worm, and the demands of worm biology will motivate the development of new techniques. Single molecule imaging in live worms will become more accessible (Li et al. 2019), and optical manipulation at single-cell or subcellular resolution (Kamei et al. 2009; Shah et al. 2017; Singhal and Shaham 2017; Hirsch et al. 2018; Mittasch et al. 2018) will give us the ability to conduct fine perturbations that are difficult to achieve by genetics alone. With sophisticated algorithms and real-time feedback to control the microscope, the line between image acquisition and image analysis will be increasingly blurred (Shah et al. 2017; Wu et al. 2021), and image enhancement techniques will allow us to distill much needed information from labels that are currently considered too weak or too coarse (Guo et al. 2020; Weigert et al. 2018). Finally, we envision increasing synergy with other imaging modalities such as electron microscopy (wormimage.org), ExM (Yu et al. 2020) and X-ray tomography (Ding et al. 2019) for cross-scale analysis: the invariant lineage and body plan of the worm provide a unique advantage to guide cross-modality alignment, and new techniques are greatly easing the hurdle of large-scale data acquisition for these modalities to start acquiring pseudo time series (Witvliet et al. 2021) in the wild-type as well as mutants. Microscopy in all its forms has proved to be an invaluable tool for the understanding of *C. elegans* anatomy and physiology thus far; these advances will allow us to observe, manipulate, and understand fundamental biology at finer resolution, with greater depth, and across wider timescales.

## Funding

Work in RZB lab is funded by Israel Science Foundation grants 767/20 and 3308/20. Work in ZB lab is in part supported by NIH grants to ZB (R01GM097576, R24OD016474, and TR01OD026219) and MSKCC (P30CA008748).

## Conflicts of interest

None declared.

## Literature cited

Alpi A, Pasierbek P, Gartner A, Loidl J. Genetic and cytological characterization of the recombination protein RAD-51 in *Caenorhabditis elegans*. *Chromosoma*. 2003;112(1):6–16.



- Ando R, Hama H, Yamamoto-Hino M, Mizuno H, Miyawaki A. An optical marker based on the UV-induced green-to-red photoconversion of a fluorescent protein. *Proc Natl Acad Sci U S A*. 2002;99(20):12651–12656.
- Attreed M, Saied-Santiago K, Bülow HE. Conservation of anatomically restricted glycosaminoglycan structures in divergent nematode species. *Glycobiology*. 2016;26(8):862–870. doi:10.1093/GLYCOB/CWW037.
- Audhya A, Hyndman F, McLeod IX, Maddox AS, Yates JR, Desai A, Oegema K. A complex containing the Sm protein CAR-1 and the RNA helicase CGH-1 is required for embryonic cytokinesis in *Caenorhabditis elegans*. *J Cell Biol*. 2005;171(2):267–279. doi:10.1083/jcb.200506124.
- Azuma Y, Onami S. Biologically constrained optimization based cell membrane segmentation in *C. elegans* embryos. *BMC Bioinformatics*. 2017;18(1):1–11. doi:10.1186/S12859-017-1717-6.
- Bao Z, Murray JI. Mounting *Caenorhabditis elegans* embryos for live imaging of embryogenesis. *Cold Spring Harb Protoc*. 2011;2011(9):pdb.prot065599. doi:10.1101/pdb.prot065599.
- Bao Z, Murray JI, Boyle T, Ooi SL, Sandel MJ, Waterston RH. Automated cell lineage tracing in *Caenorhabditis elegans*. *Proc Natl Acad Sci U S A*. 2006;103(8):2707–2712. doi:10.1073/pnas.0511111103.
- Belin BJ, Goins LM, Mullins RD. Comparative analysis of tools for live cell imaging of actin network architecture. *BioArchitecture*. 2014;4(6):189–202. doi:10.1080/19490992.2014.1047714.
- Bender A, Woydziak ZR, Fu L, Branden M, Zhou Z, Ackley BD, Peterson BR. Novel acid-activated fluorophores reveal a dynamic wave of protons in the intestine of *Caenorhabditis elegans*. *ACS Chem Biol*. 2013;8(3):636–642. doi:10.1021/cb300396j.
- Berg S, Kutra D, Kroeger T, Straehle CN, Kausler BX, Haubold C, Schiegg M, Ales J, Beier T, Rudy M, et al. ilastik: interactive machine learning for (bio)image analysis. *Nat Methods*. 2019;16(12):1226–1232. doi:10.1038/s41592-019-0582-9.
- Berger S, Lattmann E, Aegerter-Wilmsen T, Hengartner M, Hajnal A, deMello A, Solvas X C I. Long-term *C. elegans* immobilization enables high resolution developmental studies in vivo. *Lab Chip*. 2018;18(9):1359–1368. doi:10.1039/C7LC01185G.
- Berger S, Spiri S, deMello A, Hajnal A. Microfluidic-based imaging of complete *Caenorhabditis elegans* larval development. *Development (Cambridge)*. 2021;148(18). doi:10.1242/dev.199674
- Boothe T, Hilbert L, Heide M, Berninger L, Huttner WB, Zaburdaev V, Vastenhouw NL, Myers EW, Drechsel DN, Rink JC. A tunable refractive index matching medium for live imaging cells, tissues and model organisms. *eLife*. 2017;6:e27240. doi:10.7554/ELIFE.27240.
- Bouffard J, Cecchetelli AD, Clifford C, Sethi K, Zaidel-Bar R, Cram EJ. The RhoGAP SPV-1 regulates calcium signaling to control the contractility of the *Caenorhabditis elegans* spermatheca during embryo transits. *Mol Biol Cell*. 2019;30(7):907–922. doi:10.1091/mbc.E18-10-0633.
- Boulin T, Etchberger JF, Hobert O. Reporter gene fusions. In: *WormBook: The Online Review of C. elegans Biology*. 2006;1–23. doi:10.1895/WORMBOOK.1.106.1.
- Boyle TJ, Bao Z, Murray JI, Araya CL, Waterston RH. AceTree: a tool for visual analysis of *Caenorhabditis elegans* embryogenesis. *BMC Bioinformatics*. 2006;7(1):275. doi:10.1186/1471-2105-7-275.
- Breimann L, Preusser F, Preibisch S. Light-microscopy methods in *C. elegans* research. *Curr Opin Syst Biol*. 2019;13:82–92. doi:10.1016/j.COISB.2018.11.004.
- Carmi I, Kopczynski JB, Meyer BJ. The nuclear hormone receptor SEX-1 is an X-chromosome signal that determines nematode sex. *Nature*. 1998;396(6707):168–173. doi:10.1038/24164.
- Carranza N, Smal I, Dzyubachyk O, Niessen W, Meijering E. Automated lineage tree reconstruction from *Caenorhabditis elegans* image data using particle filtering based cell tracking. *Proc Int Symp Biomed Imaging*. 2011;1921–1924. doi:10.1109/ISBI.2011.5872785.
- Chai Y, Li W, Feng G, Yang Y, Wang X, Ou G. Live imaging of cellular dynamics during *Caenorhabditis elegans* postembryonic development. *Nat Protoc*. 2012;7(12):2090–2102. doi:10.1038/nprot.2012.128.
- Chalfie M, Tu Y, Euskirchen G, Ward WW, Prasher DC. Green fluorescent protein as a marker for gene expression. *Science (New York, NY)*. 1994;263(5148):802–805.
- Chen C, Fenk LA, De Bono M. Efficient genome editing in *Caenorhabditis elegans* by CRISPR-targeted homologous recombination. *Nucleic Acids Res*. 2013;41(20):e193. doi:10.1093/nar/gkt805.
- Chia PH, Patel MR, Shen K. NAB-1 instructs synapse assembly by linking adhesion molecules and F-actin to active zone proteins. *Nat Neurosci*. 2012;15(2):234–242. doi:10.1038/nn.2991.
- Chiu H, Schwartz HT, Antoshechkin I, Sternberg PW. Transgene-free genome editing in *Caenorhabditis elegans* using CRISPR-Cas. *Genetics*. 2013;195(3):1167–1171. doi:10.1534/genetics.113.155879.
- Bulinski JC, Odde DJ, Howell BJ, Salmon TD, Waterman-Storer CM. Rapid dynamics of the microtubule binding of ensconsin in vivo. *J Cell Sci*. 2001;114(Pt 21):3885–3897. doi:10.1242/jcs.114.21.3885.
- Cao J, Guan G, Ho VWS, Wong M-K, Chan L-Y, Tang C, Zhao Z, Yan H. Establishment of a morphological atlas of the *Caenorhabditis elegans* embryo using deep-learning-based 4D segmentation. *Nat Commun*. 2020;11(1):10.1038/s41467-020-19863-x
- Choi W, Fang-Yen C, Badizadegan K, Oh S, Lue N, Dasari RR, Feld MS. Tomographic phase microscopy. *Nat Methods*. 2007;4(9):717–719. doi:10.1038/nmeth1078.
- Christensen RP, Bokinsky A, Santella A, Wu Y, Marquina-Solis J, Guo M, Kovacevic I, Kumar A, Winter PW, Tashakkori N, et al. Untwisting the *Caenorhabditis elegans* embryo. *eLife*. 2015;4. doi:10.7554/ELIFE.10070.
- Chung SH, Sun L, Gabel CV. In vivo neuronal calcium imaging in *C. elegans*. *J Vis Evol*. 2013;74(74). doi:10.3791/50357.
- Churgin MA, Jung SK, Yu CC, Chen X, Raizen DM, Fang-Yen C. Longitudinal imaging of *Caenorhabditis elegans* in a microfabricated device reveals variation in behavioral decline during aging. *eLife*. 2017;6:e26652. doi:10.7554/ELIFE.26652.
- Cizeron M, Granger L, Bülow HE, Bessereau J-L. Specific heparan sulfate modifications stabilize the synaptic organizer MADD-4/Punctin at *Caenorhabditis elegans* neuromuscular junctions. *Genetics*. 2021;218(4). doi:10.1093/GENETICS/TYAB073.
- Collins TJ. ImageJ for microscopy. *Biotechniques*. 2007;43(1 Suppl):25–30. http://www.ncbi.nlm.nih.gov/pubmed/17936939.
- de Chaumont F, Dallongeville S, Chenouard N, Hervé N, Pop S, Provoost T, Meas-Yedid V, Pankajakshan P, Lecomte T, Le Montagner Y, et al. Icy: an open bioimage informatics platform for extended reproducible research. *Nat Methods*. 2012;9(7):690–696. doi:10.1038/nmeth.2075.
- de la Cova C, Townley R, Regot S, Greenwald I. A real-time biosensor for ERK activity reveals signaling dynamics during *C. elegans* cell fate specification. *Dev Cell*. 2017;42(5):542–553.e4. doi:10.1016/j.DEVCEL.2017.07.014.
- Deng W, Shi X, Tjian R, Lionnet T, Singer RH. CASFISH: RISPR/Cas9-mediated in situ labeling of genomic loci in fixed cells. *Proc Natl Acad Sci U S A*. 2015;112(38):11870–11875. doi:10.1073/PNAS.1515692112.
- Devkota R, Henricsson M, Borén J, Pilon M. The *C. elegans* PAQR-2 and IGLR-2 membrane homeostasis proteins are uniquely essential for tolerating dietary saturated fats. *Biochim Biophys Acta Mol Cell Biol Lipids*. 2021;1866(4):158883. doi:10.1016/j.bbalip.2021.158883.
- Devkota R, Pilon M. FRAP: a powerful method to evaluate membrane fluidity in *Caenorhabditis elegans*. *Bio Protoc*. 2018;8(13). doi:10.21769/BIOPROTOC.2913.

- Dickinson DJ, Ward JD, Reiner DJ, Goldstein B. Engineering the *Caenorhabditis elegans* genome using Cas9-triggered homologous recombination. *Nat Methods*. 2013;10(10):1028–1034. doi: [10.1038/nmeth.2641](https://doi.org/10.1038/nmeth.2641).
- Ding WY, Ong HT, Hara Y, Wongsantichon J, Toyama Y, Robinson RC, Nédélec F, Zaidel-Bar R. Plastin increases cortical connectivity to facilitate robust polarization and timely cytokinesis. *J Cell Biol*. 2017;216(5):1371–1386. doi: [10.1083/jcb.201603070](https://doi.org/10.1083/jcb.201603070).
- Ding Y, Vanselow DJ, Yakovlev MA, Katz SR, Lin AY, Clark DP, Vargas P, Xin X, Copper JE, Canfield VA, et al. Computational 3D histological phenotyping of whole zebrafish by X-ray histotomography. *eLife*. 2019;8. doi: [10.7554/eLife.44898](https://doi.org/10.7554/eLife.44898).
- Duncan LH, Moyle MW, Shao L, Sengupta T, Ikegami R, Kumar A, Guo M, Christensen R, Santella A, Bao Z, et al. Isotropic light-sheet microscopy and automated cell lineage analyses to catalogue *Caenorhabditis elegans* embryogenesis with subcellular resolution. *J Vis Evol*. 2019;2019(148). doi: [10.3791/59533](https://doi.org/10.3791/59533).
- El Mouridi S, Lecroisey C, Tardy P, Mercier M, Leclercq-Blondel A, Zariouh N, Boulon T. Reliable CRISPR/Cas9 genome engineering in *Caenorhabditis elegans* using a single efficient sgRNA and an easily recognizable phenotype. *G3 (Bethesda)*. 2017;7(5):1429–1437. doi: [10.1534/G3.117.040824](https://doi.org/10.1534/G3.117.040824).
- Emmons SW, Yemini E, Zimmer M. Methods for analyzing neuronal structure and activity in *Caenorhabditis elegans*. *Genetics*. 2021; 218(4). doi: [10.1093/GENETICS/IYAB072](https://doi.org/10.1093/GENETICS/IYAB072).
- Fatouros C, Pir GJ, Biernat J, Koushika SP, Mandelkow E, Mandelkow E-M, Schmidt E, Baumeister R. Inhibition of tau aggregation in a novel *Caenorhabditis elegans* model of tauopathy mitigates proteotoxicity. *Hum Mol Genet*. 2012;21(16):3587–3603. doi: [10.1093/HMG/DDS190](https://doi.org/10.1093/HMG/DDS190).
- Feinberg EH, Vanhoven MK, Bendsky A, Wang G, Fetter RD, Shen K, Bargmann CI. GFP Reconstitution Across Synaptic Partners (GRASP) defines cell contacts and synapses in living nervous systems. *Neuron*. 2008;57(3):353–363. doi: [10.1016/j.neuron.2007.11.030](https://doi.org/10.1016/j.neuron.2007.11.030).
- Fields BD, Nguyen SC, Nir G, Kennedy S. A multiplexed DNA FISH strategy for assessing genome architecture in *Caenorhabditis elegans*. *eLife*. 2019;8. doi: [10.7554/eLife.42823](https://doi.org/10.7554/eLife.42823).
- Francis R, Waterston RH. Muscle cell attachment in *Caenorhabditis elegans*. *J Cell Biol*. 1991;114(3):465–479. doi: [10.1083/jcb.114.3.465](https://doi.org/10.1083/jcb.114.3.465).
- Friedland AE, Tzur YB, Esvelt KM, Colaiácovo MP, Church GM, Calarco JA. Heritable genome editing in *C. elegans* via a CRISPR-Cas9 system. *Nat Methods*. 2013;10(8):741–743. doi: [10.1038/nmeth.2532](https://doi.org/10.1038/nmeth.2532).
- Gally C, Wissler F, Zahreddine H, Quintin S, Landmann F, Labouesse M. Myosin II regulation during *C. elegans* embryonic elongation: LET-502/ROCK, MRCK-1 and PAK-1, three kinases with different roles. *Development*. 2009;136(18):3109–3119. doi: [10.1242/dev.039412](https://doi.org/10.1242/dev.039412).
- Gengyo-Ando K, Kagawa-Nagamura Y, Ohkura M, Fei X, Chen M, Hashimoto K, Nakai J. A new platform for long-term tracking and recording of neural activity and simultaneous optogenetic control in freely behaving *Caenorhabditis elegans*. *J Neurosci Methods*. 2017;286:56–68. doi: [10.1016/J.JNEUMETH.2017.05.017](https://doi.org/10.1016/J.JNEUMETH.2017.05.017).
- Giurumescu CA, Kang S, Planchon TA, Betzig E, Bloomekatz J, Yelon D, Cosman P, Chisholm AD. Quantitative semi-automated analysis of morphogenesis with single-cell resolution in complex embryos. *Development*. 2012;139(22):4271–4279. doi: [10.1242/DEV.086256](https://doi.org/10.1242/DEV.086256).
- Gómez-de-Mariscal E, García-López-de-Haro C, Ouyang W, Donati L, Lundberg E, Unser M, Muñoz-Barrutia A, Sage D. DeepImageJ: A user-friendly environment to run deep learning models in ImageJ. *BioRxiv* 799270; 2021. doi: [10.1101/799270](https://doi.org/10.1101/799270).
- Goudeau J, Sharp CS, Paw J, Savy L, Leonetti MD, York AG, Updike DL, Kenyon C, Ingaramo M. Split-wrmScarlet and split-sfGFP: tools for faster, easier fluorescent labeling of endogenous proteins in *Caenorhabditis elegans*. *Genetics*. 2021;217(4). doi: [10.1093/GENETICS/IYAB014](https://doi.org/10.1093/GENETICS/IYAB014).
- Gritti N, Kienle S, Filina O, van Zon JS. Long-term time-lapse microscopy of *C. elegans* post-embryonic development. *Nat Commun*. 2016;7(1):12500–12509. doi: [10.1038/ncomms12500](https://doi.org/10.1038/ncomms12500).
- Guo M, Li Y, Su Y, Lambert T, Nogare DD, Moyle MW, Duncan LH, Ikegami R, Santella A, Rey-Suarez I, et al. Rapid image deconvolution and multiview fusion for optical microscopy. *Nat Biotechnol*. 2020;38(11):1337–1346. doi: [10.1038/s41587-020-0560-x](https://doi.org/10.1038/s41587-020-0560-x).
- Guo ZV, Hart AC, Ramanathan S. Optical interrogation of neural circuits in *Caenorhabditis elegans*. *Nat Methods*. 2009;6(12):891–896. doi: [10.1038/nmeth.1397](https://doi.org/10.1038/nmeth.1397).
- Hamer G, Matilainen O, Holmberg CI. A photoconvertible reporter of the ubiquitin-proteasome system in vivo. *Nat Methods*. 2010;7(6): 473–478. doi: [10.1038/nmeth.1460](https://doi.org/10.1038/nmeth.1460).
- He J, Zhou R, Wu Z, Carrasco MA, Kurshan PT, Farley JE, Simon DJ, Wang G, Han B, Hao J, et al. Prevalent presence of periodic actin-spectrin-based membrane skeleton in a broad range of neuronal cell types and animal species. *Proc Natl Acad Sci U S A*. 2016; 113(21):6029–6034. doi: [10.1073/pnas.1605707113](https://doi.org/10.1073/pnas.1605707113).
- He S, Cuentas-Condori A, Miller DM. NATF (native and tissue-specific fluorescence): a strategy for bright, tissue-specific GFP labeling of native proteins in *Caenorhabditis elegans*. *Genetics*. 2019; 212(2):387–395. doi: [10.1534/GENETICS.119.302063](https://doi.org/10.1534/GENETICS.119.302063).
- Hellerer T, Axäng C, Brackmann C, Hillertz P, Pilon M, Enejder A. Monitoring of lipid storage in *Caenorhabditis elegans* using coherent anti-Stokes Raman scattering (CARS) microscopy. *Proc Natl Acad Sci U S A*. 2007;104(37):14658–14663. doi: [10.1073/PNAS.0703594104](https://doi.org/10.1073/PNAS.0703594104).
- Heppert JK, Dickinson DJ, Pani AM, Higgins CD, Steward A, Ahringer J, Kuhn JR, Goldstein B. Comparative assessment of fluorescent proteins for in vivo imaging in an animal model system. *MBoC*. 2016;27(22):3385–3394. doi: [10.1091/MB.C.E16-01-0063/ASSET/IMAGES/MEDIUM/MB.C-27-3385-G001.GIF](https://doi.org/10.1091/MB.C.E16-01-0063/ASSET/IMAGES/MEDIUM/MB.C-27-3385-G001.GIF).
- Herbette M, Robert V, Bailly A, Gely L, Feil R, Llères D, Palladino F. A role for *Caenorhabditis elegans* COMPASS in germline chromatin organization. *Cells*. 2020;9(9):2049. doi: [10.3390/CELLS9092049](https://doi.org/10.3390/CELLS9092049).
- Hermann GJ, Schroeder LK, Hieb CA, Kershner AM, Rabbitts BM, Fonarev P, Grant BD, Priess JR. Genetic analysis of lysosomal trafficking in *Caenorhabditis elegans*. *Mol Biol Cell*. 2005;16(7): 3273–3288. doi: [10.1091/MB.C.E05-01-0060](https://doi.org/10.1091/MB.C.E05-01-0060).
- Hirsch SM, Sundaramoorthy S, Davies T, Zhuravlev Y, Waters JC, Shirasu-Hiza M, Dumont J, Canman JC. FLIRT: fast local infrared thermogenetics for subcellular control of protein function. *Nat Methods*. 2018;15(11):921–923. doi: [10.1038/s41592-018-0168-y](https://doi.org/10.1038/s41592-018-0168-y).
- Hörl D, Rojas Rusak F, Preusser F, Tillberg P, Randel N, Chhetri RK, Cardona A, Keller PJ, Harz H, Leonhardt H, et al. BigStitcher: reconstructing high-resolution image datasets of cleared and expanded samples. *Nat Methods*. 2019;16(9):870–874. doi: [10.1038/s41592-019-0501-0](https://doi.org/10.1038/s41592-019-0501-0).
- Hu CD, Chinenov Y, Kerppola TK. Visualization of interactions among bZIP and Rel family proteins in living cells using bimolecular fluorescence complementation. *Mol Cell*. 2002;9(4):789–798. doi: [10.1016/S1097-2765\(02\)00496-3](https://doi.org/10.1016/S1097-2765(02)00496-3).
- Hunt-Newbury R, Viveiros R, Johnsen R, Mah A, Anastas D, Fang L, Halfnight E, Lee D, Lin J, Lorch A, et al. High-throughput in vivo analysis of gene expression in *Caenorhabditis elegans*. *PLoS Biol*. 2007;5(9):e237. doi: [10.1371/JOURNAL.PBIO.0050237](https://doi.org/10.1371/JOURNAL.PBIO.0050237).
- Hüsken K, Wiesenfahrt T, Abraham C, Windoffer R, Bossinger O, Leube RE. Maintenance of the intestinal tube in *Caenorhabditis elegans*: the role of the intermediate filament protein IFC-2. *Differentiation*. 2008;76(8):881–896. doi: [10.1111/j.1432-0436.2008.00264.x](https://doi.org/10.1111/j.1432-0436.2008.00264.x).
- Jambor H, Antonietti A, Alicea B, Audisio TL, Auer S, Bhardwaj V, Burgess SJ, Ferling I, Gazda MA, Hoepfner LH, et al. Creating clear

- and informative image-based figures for scientific publications. *PLoS Biol.* 2021;19(3):e3001161. doi:10.1371/JOURNAL.PBIO.3001161.
- Ji N, van Oudenaarden A. Single molecule fluorescent in situ hybridization (smFISH) of *C. elegans* worms and embryos. In: *WormBook: The Online Review of C. elegans Biology*. 2012;1–16. doi:10.1895/WORMBOOK.1.153.1.
- Johnson D, Nehrke K. Mitochondrial fragmentation leads to intracellular acidification in *Caenorhabditis elegans* and mammalian cells. *Mol Biol Cell.* 2010;21(13):2191–2201. doi:10.1091/MBE.E09-10-0874/ASSET/IMAGES/MEDIUM/ZMK0131094850001.JPEG.
- Jonkman J, Brown CM, Wright GD, Anderson KI, North AJ. Tutorial: guidance for quantitative confocal microscopy. *Nat Protoc.* 2020;15(5):1585–1611. doi:10.1038/s41596-020-0313-9.
- Kamei Y, Suzuki M, Watanabe K, Fujimori K, Kawasaki T, Deguchi T, Yoneda Y, Todo T, Takagi S, Funatsu T, et al. Infrared laser-mediated gene induction in targeted single cells in vivo. *Nat Methods.* 2009;6(1):79–81. doi:10.1038/nmeth.1278.
- Kaminski CF, Rees EJ, Schierle GSK. A quantitative protocol for intensity-based live cell FRET imaging. *Methods Mol Biol (Clifton, NJ).* 2014;1076:445–454. doi:10.1007/978-1-62703-649-8\_19.
- Karabinos A, Schulze E, Schünemann J, Parry DAD, Weber K. In vivo and in vitro evidence that the four essential intermediate filament (IF) proteins A1, A2, A3 and B1 of the nematode *Caenorhabditis elegans* form an obligate heteropolymeric IF system. *J Mol Biol.* 2003;333(2):307–319. doi:10.1016/j.jmb.2003.08.041.
- Katic I, Großhans H. Targeted heritable mutation and gene conversion by Cas9-CRISPR in *Caenorhabditis elegans*. *Genetics.* 2013;195(3):1173–1176. doi:10.1534/genetics.113.155754.
- Katzman B, Tang D, Santella A, Bao Z. AceTree: a major update and case study in the long term maintenance of open-source scientific software. *BMC Bioinformatics.* 2018;19(1):1–7. doi:10.1186/S12859-018-2127-0.
- Keil W, Kutscher LM, Shaham S, Siggia ED. Long-term high-resolution imaging of developing *C. elegans* larvae with microfluidics in brief. *Dev Cell.* 2017;40(2):202–214. doi:10.1016/j.devcel.2016.11.022.
- Köhler S, Wojcik M, Xu K, Dernburg AF. Superresolution microscopy reveals the three-dimensional organization of meiotic chromosome axes in intact *Caenorhabditis elegans* tissue. *Proc Natl Acad Sci U S A.* 2017;114(24):E4734–E4743. doi:10.1073/pnas.1702312114.
- Komura T, Yamanaka M, Nishimura K, Hara K, Nishikawa Y. Autofluorescence as a noninvasive biomarker of senescence and advanced glycation end products in *Caenorhabditis elegans*. *NPJ Aging Mech Dis.* 2021;7(1):12. doi:10.1038/s41514-021-00061-y.
- Koury E, Harrell K, Smolikove S. Differential RPA-1 and RAD-51 recruitment in vivo throughout the *C. elegans* germline, as revealed by laser microirradiation. *Nucleic Acids Res.* 2018;46(2):748–764. doi:10.1093/nar/gkx1243.
- Kovacevic I, Orozco JM, Cram EJ. Filamin and phospholipase C- $\epsilon$  are required for calcium signaling in the *Caenorhabditis elegans* spermatheca. *PLOS Genet.* 2013;9(5):e1003510. doi:10.1371/JOURNAL.PGEN.1003510.
- Kozłowski C, Srayko M, Nedelec F. Cortical microtubule contacts position the spindle in *C. elegans* embryos. *Cell.* 2007;129(3):499–510. doi:10.1016/j.cell.2007.03.027.
- Krieg M, Dunn AR, Goodman MB. Mechanical control of the sense of touch by  $\beta$ -spectrin. *Nat Cell Biol.* 2014;16(3):224–233. doi:10.1038/ncb2915.
- Krieg M, Stühmer J, Cueva JG, Fetter R, Spilker K, Cremers D, Shen K, Dunn AR, Goodman MB. Genetic defects in  $\beta$ -spectrin and tau sensitize *C. elegans* axons to movement-induced damage via torque-tension coupling. *eLife.* 2017;6. doi:10.7554/ELIFE.20172.
- Krull A, Buchholz T-O, Jug F. Noise2Void- Learning Denoising from Single Noisy Images. 2019. arXiv:1811.10980
- Kurshan PT, Merrill SA, Dong Y, Ding C, Hammarlund M, Bai J, Jorgensen EM, Shen K.  $\gamma$ -Neurexin and frizzled mediate parallel synapse assembly pathways antagonized by receptor endocytosis. *Neuron.* 2018;100(1):150–166.e4. doi:10.1016/j.neuron.2018.09.007.
- Lalit M, Tomancak P, Jug F. *Embedding-Based Instance Segmentation in Microscopy*. arXiv. 2021. https://arxiv.org/abs/2101.10033v2.
- Lambert TJ, Waters JC. Navigating challenges in the application of superresolution microscopy. *J Cell Biol.* 2017;216(1):53–63. doi:10.1083/JCB.201610011.
- Lant B, Derry WB. Fluorescent visualization of germline apoptosis in living *Caenorhabditis elegans*. *Cold Spring Harb Protoc.* 2014;2014(4):420–427. doi:10.1101/pdb.prot080226.
- Lantzsch I, Yu CH, Chen YZ, Zimyanin V, Yazdkhasti H, Lindow N, Szentgyoergyi E, Pani AM, Prohaska S, Srayko M, et al. Microtubule reorganization during female meiosis in *C. elegans*. *eLife.* 2021;10. doi:10.7554/ELIFE.58903.
- Lardennois A, Pásti G, Ferraro T, Llense F, Mahou P, Pontabry J, Rodriguez D, Kim S, Ono S, Beaurepaire E, et al. An actin-based viscoplastic lock ensures progressive body axis elongation. *Nature.* 2019;573(7773):266–270. doi:10.1038/S41586-019-1509-4.
- Laughlin ST, Bertozzi CR. In vivo imaging of *Caenorhabditis elegans* glycans. *ACS Chem Biol.* 2009;4(12):1068–1072. doi:10.1021/CB900254Y/SUPPL\_FILE/CB900254Y\_SI\_001.PDF.
- Le Thuc T, Duren HM, Slipchenko MN, Hu CD, Cheng JX. Label-free quantitative analysis of lipid metabolism in living *Caenorhabditis elegans*. *J Lipid Res.* 2010;51(3):672–677. doi:10.1194/JLR.D000638.
- Lee CH, Shin H, Kimble J. Dynamics of Notch-dependent transcriptional bursting in its native context. *Dev Cell.* 2019;50(4):426–435.e4. doi:10.1016/j.DEVCEL.2019.07.001.
- Lev I, Toker IA, Mor Y, Nitzan A, Weintraub G, Antonova O, Bhonkar O, Shushan I, Ben Seroussi U, Claycomb JM, Anava, et al. Germ granules govern small RNA inheritance. *Curr Biol.* 2019;29(17):2880–2891.e4. doi:10.1016/j.CUB.2019.07.054.
- Li J, Dong A, Saydaminova K, Chang H, Wang G, Ochiai H, Yamamoto T, Pertsinidis A. Single-molecule nanoscopy elucidates RNA polymerase II transcription at single genes in live cells. *Cell.* 2019;178(2):491–506.e28. doi:10.1016/j.CELL.2019.05.029.
- Li Z, Zhang P, Zhang R, Wang X, Tse YC, Zhang H. A collection of toolkit strains reveals distinct localization and dynamics of membrane-associated transcripts in epithelia. *Cell Rep.* 2021;35(5):109072. doi:10.1016/j.celrep.2021.109072.
- Liu G, Rogers J, Murphy CT, Rongo C. EGF signalling activates the ubiquitin proteasome system to modulate *C. elegans* lifespan. *EMBO J.* 2011;30(15):2990–3003. doi:10.1038/emboj.2011.195.
- Llères D, Bailly AP, Perrin A, Norman DG, Xirodimas DP, Feil R. Quantitative FLIM-FRET Microscopy to Monitor Nanoscale Chromatin Compaction In Vivo Reveals Structural Roles of Condensin Complexes. *Cell Reports.* 2017;18(7):1791–1803. doi:10.1016/j.celrep.2017.01.043
- Lo TW, Pickle CS, Lin S, Ralston EJ, Gurling M, Schartner CM, Bian Q, Doudna JA, Meyer BJ. Precise and heritable genome editing in evolutionarily diverse nematodes using TALENs and CRISPR/Cas9 to engineer insertions and deletions. *Genetics.* 2013;195(2):331–348. doi:10.1534/genetics.113.155382.
- Ma H, Naseri A, Reyes-Gutierrez P, Wolfe SA, Zhang S, Pederson T. Multicolor CRISPR labeling of chromosomal loci in human cells. *Proc Natl Acad Sci U S A.* 2015;112(10):3002–3007. doi:10.1073/PNAS.1420024112.



- Mace DL, Weisdepp P, Gevirtzman L, Boyle T, Waterston RH. A high-fidelity cell lineage tracing method for obtaining systematic spatiotemporal gene expression patterns in *Caenorhabditis elegans*. *G3* (Bethesda). 2013;3(5):851–863. doi:[10.1534/G3.113.005918](https://doi.org/10.1534/G3.113.005918).
- Maduzia LL, Yu E, Zhang Y. *Caenorhabditis elegans* galectins LEC-6 and LEC-10 interact with similar glycoconjugates in the intestine. *J Biol Chem*. 2011;286(6):4371–4381. doi:[10.1074/JBC.M110.188581](https://doi.org/10.1074/JBC.M110.188581).
- Malin-Mayor C, Hirsch P, Guignard L, McDole K, Wan Y, Lemon WC, Keller PJ, Preibisch S, Funke J. Automated reconstruction of whole-embryo cell lineages by learning from sparse annotations. *BioRxiv* 2021.07.28.454016; 2021. doi:[10.1101/2021.07.28.454016](https://doi.org/10.1101/2021.07.28.454016).
- Matilainen O, Jha S, Holmberg CI. Fluorescent tools for in vivo studies on the ubiquitin- proteasome system. *Methods Mol Biol*. 2016; 1449:215–222. doi:[10.1007/978-1-4939-3756-1\\_12](https://doi.org/10.1007/978-1-4939-3756-1_12).
- McQuin C, Goodman A, Chernyshev V, Kamensky L, Cimini BA, Karhohs KW, Doan M, Ding L, Rafelski SM, Thirstrup D, et al. CellProfiler 3.0: Next-generation image processing for biology. *PLoS Biol*. 2018;16(7):e2005970. doi:[10.1371/journal.pbio.2005970](https://doi.org/10.1371/journal.pbio.2005970).
- Mendenhall AR, Tedesco PM, Sands B, Johnson TE, Brent R. Single cell quantification of reporter gene expression in live adult *Caenorhabditis elegans* reveals reproducible cell-specific expression patterns and underlying biological variation. *PLoS One*. 2015;10(5):e0124289. doi:[10.1371/JOURNAL.PONE.0124289](https://doi.org/10.1371/JOURNAL.PONE.0124289).
- Meng F, Suchyna TM, Lazakovitch E, Gronostajski RM, Sachs F. Real time FRET based detection of mechanical stress in cytoskeletal and extracellular matrix proteins. *Cell Mol Bioeng*. 2011;4(2): 148–159. doi:[10.1007/s12195-010-0140-0](https://doi.org/10.1007/s12195-010-0140-0).
- Mittasch M, Gross P, Nestler M, Fritsch AW, Iserman C, Kar M, Munder M, Voigt A, Alberti S, Grill SW, et al. Non-invasive perturbations of intracellular flow reveal physical principles of cell organization. *Nat Cell Biol*. 2018;20(3):344–351. doi:[10.1038/s41556-017-0032-9](https://doi.org/10.1038/s41556-017-0032-9).
- Mondal S, Dubey J, Awasthi A, Sure GR, Vasudevan A, Koushika SP. Tracking mitochondrial density and positioning along a growing neuronal process in individual *C. elegans* neuron using a long-term growth and imaging microfluidic device. *eNeuro*. 2021;8(4). doi:[10.1523/ENEURO.0360-20.2021](https://doi.org/10.1523/ENEURO.0360-20.2021).
- Moore JL, Du Z, Bao Z. Systematic quantification of developmental phenotypes at single-cell resolution during embryogenesis. *Development*. 2013;140(15):3266–3274. doi:[10.1242/dev.096040](https://doi.org/10.1242/dev.096040).
- Mosquera JV, Bacher MC, Priess JR. Nuclear lipid droplets and nuclear damage in *Caenorhabditis elegans*. *PLoS Genet*. 2021;17(6): e1009602. doi:[10.1371/JOURNAL.PGEN.1009602](https://doi.org/10.1371/JOURNAL.PGEN.1009602).
- Mota AAR, Correa JR, de Andrade LP, Assumpção JAF, de Souza Cintra GA, Freitas-Junior LH, da Silva WA, de Oliveira HCB, Neto BAD. From live cells to *Caenorhabditis elegans*: selective staining and quantification of lipid structures using a fluorescent hybrid benzothiadiazole derivative. *ACS Omega*. 2018;3(4):3874–3881. doi:[10.1021/acsomega.8b00434](https://doi.org/10.1021/acsomega.8b00434).
- Motley AM, Hetteema EH, Ketting R, Plasterk R, Tabak HF. *Caenorhabditis elegans* has a single pathway to target matrix proteins to peroxisomes. *EMBO Rep*. 2000;1(1):40–46. doi:[10.1093/embo-reports/kvd010](https://doi.org/10.1093/embo-reports/kvd010).
- Nance J, Frøkjær-Jensen C. The *Caenorhabditis elegans* transgenic toolbox. *Genetics*. 2019;212(4):959–990. doi:[10.1534/GENETICS.119.301506](https://doi.org/10.1534/GENETICS.119.301506).
- Napari Contributors. Napari: A Multi-dimensional Image Viewer for Python; 2019. doi:[10.5281/zenodo.3555620](https://doi.org/10.5281/zenodo.3555620).
- Nguyen JP, Shipley FB, Linder AN, Plummer GS, Liu M, Setru SU, Shaevitz JW, Leifer AM. Whole-brain calcium imaging with cellular resolution in freely behaving *Caenorhabditis elegans*. *Proc Natl Acad Sci U S A*. 2016;113(8):E1074–E1081. doi:[10.1073/PNAS.1507110112](https://doi.org/10.1073/PNAS.1507110112).
- O'Rourke EJ, Soukas AA, Carr CE, Ruvkun G. *C. elegans* major fats are stored in vesicles distinct from lysosome-related organelles. *Cell Metab*. 2009;10(5):430–435. doi:[10.1016/J.CMET.2009.10.002](https://doi.org/10.1016/J.CMET.2009.10.002).
- Oegema K, Desai A, Rybina S, Kirkham M, Hyman AA. Functional analysis of kinetochore assembly in *Caenorhabditis elegans*. *J Cell Biol*. 2001;153(6):1209–1226. doi:[10.1083/jcb.153.6.1209](https://doi.org/10.1083/jcb.153.6.1209).
- Okkema PG, Krause M. Transcriptional regulation. In: *WormBook: The Online Review of C. elegans Biology*, 2005;1–40. doi:[10.1895/WORMBOOK.1.45.1](https://doi.org/10.1895/WORMBOOK.1.45.1).
- Ou G, Stuurman N, D'Ambrosio M, Vale RD. Polarized myosin produces unequal-size daughters during asymmetric cell division. *Science*. 2010;330(6004):677–680. doi:[10.1126/science.1196112](https://doi.org/10.1126/science.1196112).
- Papandreou ME, Palikaras K, Tavernarakis N. Assessment of de novo protein synthesis rates in *Caenorhabditis elegans*. *J Vis Evol*. 2020; 163:e61170. doi:[10.3791/61170](https://doi.org/10.3791/61170).
- Phillips CM, Montgomery TA, Breen PC, Ruvkun G. MUT-16 promotes formation of perinuclear mutator foci required for RNA silencing in the *C. elegans* germline. *Genes Dev*. 2012;26(13):1433–1444. doi:[10.1101/gad.193904.112](https://doi.org/10.1101/gad.193904.112).
- Pietzsch T, Saalfeld S, Preibisch S, Tomancak P. BigDataViewer: visualization and processing for large image data sets. *Nat Methods*. 2015;12(6):481–483. doi:[10.1038/nmeth.3392](https://doi.org/10.1038/nmeth.3392).
- Pincus Z, Mazer TC, Slack FJ. Autofluorescence as a measure of senescence in *C. elegans*: look to red, not blue or green. *Aging (Albany, NY)*. 2016;8(5):889–898. doi:[10.18632/aging.100936](https://doi.org/10.18632/aging.100936).
- Pohl C, Bao Z. Chiral forces organize left-right patterning in *C. elegans* by uncoupling midline and anteroposterior axis. *Dev Cell*. 2010; 19(3):402–412. doi:[10.1016/j.devcel.2010.08.014](https://doi.org/10.1016/j.devcel.2010.08.014).
- Poteryaev D, Squirrell JM, Campbell JM, White JG, Spang A. Involvement of the actin cytoskeleton and homotypic membrane fusion in ER dynamics in *Caenorhabditis elegans*. *Mol Biol Cell*. 2005;16(5):2139–2153. doi:[10.1091/MBE.E04-08-0726/ASSET/IMAGES/MEDIUM/ZMK0050531400001.JPEG](https://doi.org/10.1091/MBE.E04-08-0726/ASSET/IMAGES/MEDIUM/ZMK0050531400001.JPEG).
- Power RM, Huisken J. A guide to light-sheet fluorescence microscopy for multiscale imaging. *Nat Methods*. 2017;14(4):360–373. doi:[10.1038/nmeth.4224](https://doi.org/10.1038/nmeth.4224).
- Poyurovsky MV, Jacq X, Ma C, Karni-Schmidt O, Parker PJ, Chalfie M, Manley JL, Prives C. Nucleotide binding by the MDM2 RING domain facilitates Arf-independent MDM2 nucleolar localization. *Mol Cell*. 2003;12(4):875–887. doi:[10.1016/S1097-2765\(03\)00400-3](https://doi.org/10.1016/S1097-2765(03)00400-3).
- Prakash M, Lalit M, Tomancak P, Krul A, Jug F. Fully Unsupervised Probabilistic Noise2Void. In: *2020 IEEE 17th International Symposium on Biomedical Imaging (ISBI)*; 2020. p. 154–158. doi:[10.1109/ISBI45749.2020.9098612](https://doi.org/10.1109/ISBI45749.2020.9098612).
- Preibisch S, Saalfeld S, Schindelin J, Tomancak P. Software for bead-based registration of selective plane illumination microscopy data. *Nat Methods*. 2010;7(6):418–419. doi:[10.1038/nmeth.0610-418](https://doi.org/10.1038/nmeth.0610-418).
- Priti A, Ong HT, Toyama Y, Padmanabhan A, Dasgupta S, Krajnc M, Zaidel-Bar R. Syncytial germline architecture is actively maintained by contraction of an internal actomyosin corset. *Nat Commun*. 2018;9(1). doi:[10.1038/s41467-018-07149-2](https://doi.org/10.1038/s41467-018-07149-2).
- Qadota H, Matsunaga Y, Nguyen KCQ, Mattheyses A, Hall DH, Benian GM. High-resolution imaging of muscle attachment structures in *Caenorhabditis elegans*. *Cytoskeleton (Hoboken)*. 2017;74(11):426–442. doi:[10.1002/CM.21410](https://doi.org/10.1002/CM.21410).
- Raj A, van den Bogaard P, Rifkin SA, van Oudenaarden A, Tyagi S. Imaging individual mRNA molecules using multiple singly labeled probes. *Nat Methods*. 2008;5(10):877–879. doi:[10.1038/nmeth.1253](https://doi.org/10.1038/nmeth.1253).
- Rankin BR, Moneron G, Wurm CA, Nelson JC, Walter A, Schwarzer D, Schroeder J, Colón-Ramos DA, Hell SW. Nanoscopy in a living

- multicellular organism expressing GFP. *Biophys J.* 2011;100(12):L63–L65. doi:[10.1016/j.bpj.2011.05.020](https://doi.org/10.1016/j.bpj.2011.05.020).
- van Rijnberk LM, van der Horst SEM, van den Heuvel S, Ruijtenberg S. A dual transcriptional reporter and CDK-activity sensor marks cell cycle entry and progression in *C. elegans*. *PLoS One.* 2017;12(2):e0171600. doi:[10.1371/JOURNAL.PONE.0171600](https://doi.org/10.1371/JOURNAL.PONE.0171600).
- Rohde CB, Yanik MF. Subcellular in vivo time-lapse imaging and optical manipulation of *Caenorhabditis elegans* in standard multiwell plates. *Nat Commun.* 2011;2(1):1–7. doi:[10.1038/ncomms1266](https://doi.org/10.1038/ncomms1266).
- Royer LA, Weigert M, Günther U, Maghelli N, Jug F, Sbalzarini IF, Myers EW. ClearVolume: open-source live 3D visualization for light-sheet microscopy. *Nat Methods.* 2015;12(6):480–481. doi:[10.1038/nmeth.3372](https://doi.org/10.1038/nmeth.3372).
- Sage D, Donati L, Soulez F, Fortun D, Schmit G, Seitz A, Guet R, Vonesch C, Unser M. DeconvolutionLab2: an open-source software for deconvolution microscopy. *Methods.* 2017;115:28–41. doi:[10.1016/j.ymeth.2016.12.015](https://doi.org/10.1016/j.ymeth.2016.12.015).
- Santella A, Catena R, Kovacevic I, Shah P, Yu Z, Marquina-Solis J, Kumar A, Wu Y, Schaff J, Colón-Ramos D, et al. WormGUIDES: an interactive single cell developmental atlas and tool for collaborative multidimensional data exploration. *BMC Bioinformatics.* 2015;16(1):189. doi:[10.1186/s12859-015-0627-8](https://doi.org/10.1186/s12859-015-0627-8).
- Santella A, Du Z, Bao Z, Bischoff M, Parfitt D, Zernicka-Goetz M, Keller P, Schmidt A, Wittbrodt J, Stelzer E, et al. A semi-local neighborhood-based framework for probabilistic cell lineage tracing. *BMC Bioinformatics.* 2014;15(1):217. doi:[10.1186/1471-2105-15-217](https://doi.org/10.1186/1471-2105-15-217).
- Santella A, Du Z, Nowotschin S, Hadjantonakis A-K, Bao Z. A hybrid blob-slice model for accurate and efficient detection of fluorescence labeled nuclei in 3D. *BMC Bioinformatics.* 2010;11(1):580. doi:[10.1186/1471-2105-11-580](https://doi.org/10.1186/1471-2105-11-580).
- Sato K, Norris A, Sato M, Grant BD. *C. elegans* as a model for membrane traffic. In: *WormBook: The Online Review of C. elegans Biology.* 2014;1–47. doi:[10.1895/wormbook.1.77.2](https://doi.org/10.1895/wormbook.1.77.2).
- Schindelin J, Arganda-Carreras I, Frise E, Kaynig V, Longair M, Pietzsch T, Preibisch S, Rueden C, Saalfeld S, Schmid B, et al. Fiji: an open-source platform for biological-image analysis. *Nat Methods.* 2012;9(7):676–682. doi:[10.1038/nmeth.2019](https://doi.org/10.1038/nmeth.2019).
- Schnabel R, Hutter H, Moerman D, Schnabel H. Assessing normal embryogenesis in *Caenorhabditis elegans* using a 4D microscope: variability of development and regional specification. *Dev Biol.* 1997;184(2):234–265. doi:[10.1006/dbio.1997.8509](https://doi.org/10.1006/dbio.1997.8509).
- Schwarz J, Spies J-P, Bringmann H. Reduced muscle contraction and a relaxed posture during sleep-like Lethargus. *Worm.* 2012;1(1):12–14. doi:[10.4161/WORM.19499](https://doi.org/10.4161/WORM.19499).
- Sengupta T, Koonce NL, Vázquez-Martínez N, Moyle MW, Duncan LH, Emerson SE, Han X, Shao L, Wu Y, Santella A, et al. Differential adhesion regulates neurite placement via a retrograde zipper mechanism. *eLife.* 2021;10. doi:[10.7554/ELIFE.71171](https://doi.org/10.7554/ELIFE.71171)
- Shaffer JM, Greenwald I. SALSA, a genetically encoded biosensor for spatiotemporal quantification of Notch signal transduction in vivo. *Developmental Cell.* 2022;57(7):930–944.e6. doi:[10.1016/j.devcel.2022.03.008](https://doi.org/10.1016/j.devcel.2022.03.008)
- Shah PK, Santella A, Jacobo A, Siletti K, Hudspeth AJ, Bao Z. An in toto approach to dissecting cellular interactions in complex tissues. *Dev Cell.* 2017;43(4):530–540.e4. doi:[10.1016/j.DEVCEL.2017.10.021](https://doi.org/10.1016/j.DEVCEL.2017.10.021).
- Shidara H, Hotta K, Oka K. Compartmentalized cGMP Responses of Olfactory Sensory Neurons in *Caenorhabditis elegans*. *J Neurosci.* 2017;37(14):3753–3763. doi:[10.1523/JNEUROSCI.2628-16.2017](https://doi.org/10.1523/JNEUROSCI.2628-16.2017).
- Shinkai Y, Kuramochi M, Doi M. A simple method for visualization of locus-specific H4K20me1 modifications in living *Caenorhabditis elegans* single cells. *G3 (Bethesda).* 2018;8(7):2249–2255. doi:[10.1534/g3.118.200333](https://doi.org/10.1534/g3.118.200333).
- Singhal A, Shaham S. Infrared laser-induced gene expression for tracking development and function of single *C. elegans* embryonic neurons. *Nat Commun.* 2017;8:14100. doi:[10.1038/ncomms14100](https://doi.org/10.1038/ncomms14100).
- Spencer SL, Cappell SD, Tsai F-C, Overton KW, Wang CL, Meyer T. The proliferation-quiescence decision is controlled by a bifurcation in CDK2 activity at mitotic exit. *Cell.* 2013;155(2):369–383. doi:[10.1016/j.cell.2013.08.062](https://doi.org/10.1016/j.cell.2013.08.062).
- Spiri S, Berger S, Mereu L, DeMello A, Hajnal A. Reciprocal EGFR signaling in the anchor cell ensures precise inter-organ connection during *Caenorhabditis elegans* vulval morphogenesis. *Development (Cambridge, England).* 2022;149(1). doi:[10.1242/DEV.199900/VIDEO-8](https://doi.org/10.1242/DEV.199900/VIDEO-8).
- Spracklen AJ, Fagan TN, Lovander KE, Tootle TL. The pros and cons of common actin labeling tools for visualizing actin dynamics during *Drosophila* oogenesis. *Dev Biol.* 2014;393(2):209–226. doi:[10.1016/j.ydbio.2014.06.022](https://doi.org/10.1016/j.ydbio.2014.06.022).
- Strome S, Powers J, Dunn M, Reese K, Malone CJ, White J, Seydoux G, Saxton W. Spindle dynamics and the role of gamma-tubulin in early *Caenorhabditis elegans* embryos. *Mol Biol Cell.* 2001;12(6):1751–1764. doi:[10.1091/mbc.12.6.1751](https://doi.org/10.1091/mbc.12.6.1751).
- Sulston JE, Horvitz HR. Post-embryonic cell lineages of the nematode, *Caenorhabditis elegans*. *Dev Biol.* 1977;56(1):110–156. <http://www.ncbi.nlm.nih.gov/pubmed/838129>.
- Sulston JE, Schierenberg E, White JG, Thomson JN. The embryonic cell lineage of the nematode *Caenorhabditis elegans*. *Dev Biol.* 1983;100(1):64–119. <http://www.ncbi.nlm.nih.gov/pubmed/6684600>.
- Suzuki M, Sakashita T, Funayama T. Immobilization of live *Caenorhabditis elegans* individuals using an ultra-thin polydimethylsiloxane microfluidic chip with water retention. *J Vis Evol.* 2019;145(145). doi:[10.3791/59008](https://doi.org/10.3791/59008).
- Swedlow JR. Quantitative Fluorescence Microscopy and Image Deconvolution; 2013. p. 407–426. doi:[10.1016/B978-0-12-407761-4.00017-8](https://doi.org/10.1016/B978-0-12-407761-4.00017-8).
- Tegha-Dunghu J, Gusnowski EM, Srayko M. Measuring microtubule growth and gliding in *Caenorhabditis elegans* embryos. *Methods Mol Biol (Clifton, NJ).* 2014;1136:103–116. doi:[10.1007/978-1-4939-0329-0\\_7](https://doi.org/10.1007/978-1-4939-0329-0_7).
- Teuscher AC, Ewald CY. Overcoming autofluorescence to assess GFP expression during normal physiology and aging in *Caenorhabditis elegans*. *Bio-Protoc.* 2018;8(14). doi:[10.21769/BioProtoc.2940](https://doi.org/10.21769/BioProtoc.2940).
- Theer P, Mongis C, Knop M. PSFj: know your fluorescence microscope. *Nat Methods.* 2014;11(10):981–982. doi:[10.1038/nmeth.3102](https://doi.org/10.1038/nmeth.3102).
- Thomas BJ, Wight IE, Chou WYY, Moreno M, Dawson Z, Homayouni A, Huang H, Kim H, Jia H, Buland JR, et al. CemOrange2 fusions facilitate multifluorophore subcellular imaging in *C. elegans*. *PLoS One.* 2019;14(3):e0214257. doi:[10.1371/journal.pone.0214257](https://doi.org/10.1371/journal.pone.0214257).
- Tian L, Hires SA, Mao T, Huber D, Chiappe ME, Chalasani SH, Petreanu L, Akerboom J, McKinney SA, Schreiter ER, et al. Imaging neural activity in worms, flies and mice with improved GCaMP calcium indicators. *Nat Methods.* 2009;6(12):875–881. doi:[10.1038/NMETH.1398](https://doi.org/10.1038/NMETH.1398).
- Tse YC, Werner M, Longhini KM, Labbe J-C, Goldstein B, Glotzer M. RhoA activation during polarization and cytokinesis of the early *Caenorhabditis elegans* embryo is differentially dependent on NOP-1 and CYK-4. *Mol Biol Cell.* 2012;23(20):4020–4031. doi:[10.1091/mbc.E12-04-0268](https://doi.org/10.1091/mbc.E12-04-0268).
- Tsuyama T, Kishikawa J, Han Y-W, Harada Y, Tsubouchi A, Noji H, Kakizuka A, Yokoyama K, Uemura T, Imamura H. In vivo fluorescent adenosine 5'-triphosphate (ATP) imaging of *Drosophila*

- melanogaster* and *Caenorhabditis elegans* by using a genetically encoded fluorescent ATP biosensor optimized for low temperatures. *Anal Chem.* 2013;85(16):7889–7896. doi:[10.1021/ac4015325](https://doi.org/10.1021/ac4015325).
- Tzur YB, Friedland AE, Nadarajan S, Church GM, Calarco JA, Colaiácovo MP. Heritable custom genomic modifications in *Caenorhabditis elegans* via a CRISPR-Cas9 system. *Genetics.* 2013;195(3):1181–1185. doi:[10.1534/genetics.113.156075](https://doi.org/10.1534/genetics.113.156075).
- Vangindertael J, Beets I, Rocha S, Dedecker P, Schoofs L, Vanhoorelbeke K, Vanhoorelbeeke K, Hofkens J, Mizuno H. Super-resolution mapping of glutamate receptors in *C. elegans* by confocal correlated PALM. *Sci Rep.* 2015;5(1):13532. doi:[10.1038/srep13532](https://doi.org/10.1038/srep13532).
- Velarde N, Gunsalus KC, Piano F. Diverse roles of actin in *C. elegans* early embryogenesis. *BMC Dev Biol.* 2007;7(1):142. doi:[10.1186/1471-213X-7-142](https://doi.org/10.1186/1471-213X-7-142).
- Venkatachalam V, Ji N, Wang X, Clark C, Mitchell JK, Klein M, Tabone CJ, Florman J, Ji H, Greenwood J, et al. Pan-neuronal imaging in roaming *Caenorhabditis elegans*. *Proc Natl Acad Sci U S A.* 2016;113(8):E1082–E1088. doi:[10.1073/PNAS.1507109113/SUPPL\\_FILE/PNAS.1507109113.SM02.MP4](https://doi.org/10.1073/PNAS.1507109113/SUPPL_FILE/PNAS.1507109113.SM02.MP4).
- Voleti V, Patel KB, Li W, Perez Campos C, Bharadwaj S, Yu H, Ford C, Casper MJ, Yan RW, Liang W, et al. Real-time volumetric microscopy of in vivo dynamics and large-scale samples with SCAPE 2.0. *Nat Methods.* 2019;16(10):1054–1062. doi:[10.1038/s41592-019-0579-4](https://doi.org/10.1038/s41592-019-0579-4).
- Waaijers S, Muñoz J, Berends C, Ramalho JJ, Goerdayal SS, Low TY, Zoumaro-Djayoon AD, Hoffmann M, Koorman T, Tas RP, et al. A tissue-specific protein purification approach in *Caenorhabditis elegans* identifies novel interaction partners of DLG-1/Discs large. *BMC Biol.* 2016;14(1). doi:[10.1186/S12915-016-0286-X](https://doi.org/10.1186/S12915-016-0286-X).
- Waaijers S, Portegijs V, Kerver J, Lemmens BBLG, Tijsterman M, van den Heuvel S, Boxem M. CRISPR/Cas9-targeted mutagenesis in *Caenorhabditis elegans*. *Genetics.* 2013;195(3):1187–1191. doi:[10.1534/genetics.113.156299](https://doi.org/10.1534/genetics.113.156299).
- Wählby C, Kamensky L, Liu ZH, Riklin-Raviv T, Conery AL, O'Rourke EJ, Sokolnicki KL, Visvikis O, Ljosa V, Irazoqui JE, et al. An image analysis toolbox for high-throughput *C. elegans* assays. *Nat Methods.* 2012;9(7):714–716. doi:[10.1038/nmeth.1984](https://doi.org/10.1038/nmeth.1984).
- Wan G, Fields BD, Spracklin G, Shukla A, Phillips CM, Kennedy S. Spatiotemporal regulation of liquid-like condensates in epigenetic inheritance. *Nature.* 2018;557(7707):679–683. doi:[10.1038/s41586-018-0132-0](https://doi.org/10.1038/s41586-018-0132-0).
- Wang JT, Smith J, Chen BC, Schmidt H, Rasoloson D, Paix A, Lambrus BG, Calidas D, Betzig E, Seydoux G. Regulation of RNA granule dynamics by phosphorylation of serine-rich, intrinsically disordered proteins in *C. elegans*. *eLife.* 2014;3. Doi:[10.7554/ELIFE.04591](https://doi.org/10.7554/ELIFE.04591).
- Wang S, Hazelrigg T. Implications for bcd mRNA localization from spatial distribution of exu protein in *Drosophila* oogenesis. *Nature.* 1994;369(6479):400–403. doi:[10.1038/369400a0](https://doi.org/10.1038/369400a0).
- Waters JC. Accuracy and precision in quantitative fluorescence microscopy. *J Cell Biol.* 2009;185(7):1135–1148. doi:[10.1083/jcb.200903097](https://doi.org/10.1083/jcb.200903097).
- Weigert M, Schmidt U, Boothe T, Müller A, Dibrov A, Jain A, Wilhelm B, Schmidt D, Broaddus C, Culley S, et al. Content-aware image restoration: pushing the limits of fluorescence microscopy. *Nat Methods.* 2018;15(12):1090–1097. doi:[10.1038/s41592-018-0216-7](https://doi.org/10.1038/s41592-018-0216-7).
- Weigert M, Schmidt U, Haase R, Sugawara K, Myers G. Star-convex Polyhedra for 3D Object Detection and Segmentation in Microscopy, in *The IEEE Winter Conference on Applications of Computer Vision (WACV)*, Snowmass Village, Colorado 2020. doi:[10.1109/WACV45572.2020.9093435](https://doi.org/10.1109/WACV45572.2020.9093435).
- White JG, Amos WB, Fordham M. An evaluation of confocal versus conventional imaging of biological structures by fluorescence light microscopy. *J Cell Biol.* 1987;105(1):41–48. doi:[10.1083/jcb.105.1.41](https://doi.org/10.1083/jcb.105.1.41).
- Witvliet D, Mulcahy B, Mitchell JK, Meirovitch Y, Berger DR, Wu Y, Liu Y, Koh WX, Parvathala R, Holmyard D, et al. Connectomes across development reveal principles of brain maturation. *Nature.* 2021;596(7871):257–261. doi:[10.1038/s41586-021-03778-8](https://doi.org/10.1038/s41586-021-03778-8).
- Woldemariam S, Nagpal J, Hill T, Li J, Schneider MW, Shankar R, Futey M, Varshney A, Ali N, Mitchell J, et al. Using a robust and sensitive GFP-based cGMP sensor for real-time imaging in intact *Caenorhabditis elegans*. *Genetics.* 2019;213(1):59–77. doi:[10.1534/genetics.119.302392](https://doi.org/10.1534/genetics.119.302392).
- Wu Y, Han X, Su Y, Glidewell M, Daniels JS, Liu J, Sengupta T, Rey-Suarez I, Fischer R, Patel A, et al. Multiview confocal super-resolution microscopy. *Nature.* 2021;600(7888):279–276. doi:[10.1038/s41586-021-04110-0](https://doi.org/10.1038/s41586-021-04110-0).
- Wu Y, Shroff H. Faster, sharper, and deeper: structured illumination microscopy for biological imaging. *Nat Methods.* 2018;15(12):1011–1019. doi:[10.1038/s41592-018-0211-z](https://doi.org/10.1038/s41592-018-0211-z).
- Wu Y, Wawrzusin P, Senseney J, Fischer RS, Christensen R, Santella A, York AG, Winter PW, Waterman CM, Bao Z, et al. Spatially isotropic four-dimensional imaging with dual-view plane illumination microscopy. *Nat Biotechnol.* 2013;31(11):1032–1038. doi:[10.1038/nbt.2713](https://doi.org/10.1038/nbt.2713).
- Wühr M, Obholzer ND, Megason SG, Detrich HW, Mitchison TJ. Live imaging of the cytoskeleton in early cleavage-stage zebrafish embryos. *Methods Cell Biol.* 2011;101:1–18. doi:[10.1016/B978-0-12-387036-0.00001-3](https://doi.org/10.1016/B978-0-12-387036-0.00001-3).
- Yang TT, Kain SR, Kitts P, Kondepudi A, Yang MM, Youvan DC. Dual color microscopic imagery of cells expressing the green fluorescent protein and a red-shifted variant. *Gene.* 1996;173(1):19–23. doi:[10.1016/0378-1119\(95\)00781-4](https://doi.org/10.1016/0378-1119(95)00781-4).
- Yemini E, Lin A, Nejatbakhsh A, Varol E, Sun R, Mena GE, Samuel ADT, Paninski L, Venkatachalam V, Hobert O. NeuroPAL: a multi-color atlas for whole-brain neuronal identification in *C. elegans*. *Cell.* 2021;184(1):272–288.e11. doi:[10.1016/J.CELL.2020.12.012](https://doi.org/10.1016/J.CELL.2020.12.012).
- York AG, Chandris P, Nogare DD, Head J, Wawrzusin P, Fischer RS, Chitnis A, Shroff H. Instant super-resolution imaging in live cells and embryos via analog image processing. *Nat Methods.* 2013;10(11):1122–1130. doi:[10.1038/nmeth.2687](https://doi.org/10.1038/nmeth.2687).
- Yu C-C(J), Barry NC, Wassie AT, Sinha A, Bhattacharya A, Asano S, Zhang C, Chen F, Hobert O, Goodman MB, et al. Expansion microscopy of *C. elegans*. *eLife.* 2020;9. Doi:[10.7554/eLife.46249](https://doi.org/10.7554/eLife.46249).
- Zdinak LA, Greenberg IB, Szewczyk NJ, Barmada SJ, Cardamone-Rayner M, Hartman JJ, Jacobson LA. Transgene-coded chimeric proteins as reporters of intracellular proteolysis: starvation-induced catabolism of a lacZ Fusion protein in muscle cells of *Caenorhabditis elegans*. *J Cell Biochem.* 1997;67(1):143–153.
- Zhao Y, Araki S, Wu J, Teramoto T, Chang Y-F, Nakano M, Abdelfattah AS, Fujiwara M, Ishihara T, Nagai T, et al. An expanded palette of genetically encoded Ca<sup>2+</sup> indicators. *Science.* 2011;333(6051):1888–1891. doi:[10.1126/science.1208592](https://doi.org/10.1126/science.1208592).
- Zhou Z, Hartwig E, Horvitz HR. CED-1 is a transmembrane receptor that mediates cell corpse engulfment in *C. elegans*. *Cell.* 2001;104(1):43–56. doi:[10.1016/S0092-8674\(01\)00190-8](https://doi.org/10.1016/S0092-8674(01)00190-8).